

DTIC FILE COPY

GL-TR-89-0147

AD-A219 370

4

Measurements of High Frequency Seismic Waves

William H. Menke

Lamont-Doherty Geological Observatory
of Columbia University
Route 9W
Palisades, New York 10964

4 December 1989

Final Report
16 March 1987 - 13 March 1989

APPROVED FOR PUBLIC RELEASE; DISTRIBUTION UNLIMITED

GEOFYSICS LABORATORY
AIR FORCE SYSTEMS COMMAND
UNITED STATES AIR FORCE
HANSOM AIR FORCE BASE, MASSACHUSETTS 01731-5000

DTIC
ELECTE
MAR 20 1990
S B D

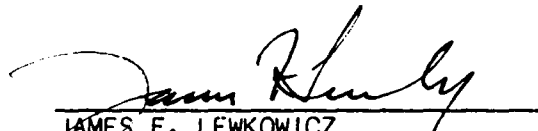
90 03 20 125


SPONSORED BY
Defense Advanced Research Projects Agency
Nuclear Monitoring Research Office
ARPA ORDER NO. 5299

MONITORED BY
Geophysics Laboratory
Contract No. F19628-87-K-0011

The views and conclusions contained in this document are those of the authors and should not be interpreted as representing the official policies, either expressed or implied, of the Defense Advanced Research Projects Agency or the U.S. Government.

This technical report has been reviewed and is approved for publication.


JAMES F. LEWKOWICZ
Contract Manager
Solid Earth Geophysics Branch
Earth Sciences Division


JAMES F. LEWKOWICZ
Branch Chief
Solid Earth Geophysics Branch
Earth Sciences Division

FOR THE COMMANDER


DONALD H. ECKHARDT, Director
Earth Sciences Division

This report has been reviewed by the ESD Public Affairs Office (PA) and is releasable to the National Technical Information Service (NTIS).

Qualified requestors may obtain additional copies from the Defense Technical Information Center. All others should apply to the National Technical Information Service.

If your address has changed, or if you wish to be removed from the mailing list, or if the addressee is no longer employed by your organization, please notify AFGL/DAA, Hanscom AFB, MA 01731-5000. This will assist us in maintaining a current mailing list.

Do not return copies of this report unless contractual obligations or notices on a specific document requires that it be returned.

REPORT DOCUMENTATION PAGE

1a REPORT SECURITY CLASSIFICATION Unclassified			1b RESTRICTIVE MARKINGS.		
2a SECURITY CLASSIFICATION AUTHORITY			3 DISTRIBUTION/AVAILABILITY OF REPORT Approved for public release. Distribution unlimited.		
2b DECLASSIFICATION/DOWNGRADING SCHEDULE					
4 PERFORMING ORGANIZATION REPORT NUMBER(S)			5 MONITORING ORGANIZATION REPORT NUMBER(S) GL-TR-89-0147		
6a NAME OF PERFORMING ORGANIZATION Lamont-Doherty Geological Observatory of Columbia Univ.		6b OFFICE SYMBOL (If applicable)		7a NAME OF MONITORING ORGANIZATION Geophysics Laboratory	
6c ADDRESS (City, State, and ZIP Code) Route 9W Palisades, New York 10964			7b ADDRESS (City, State, and ZIP Code) Hanscom Air Force Base Massachusetts 01731-5000		
8a NAME OF FUNDING/SPONSORING ORGANIZATION DARPA		8b OFFICE SYMBOL (If applicable) NMRO		9 PROCUREMENT INSTRUMENT IDENTIFICATION NUMBER F19628-87-K-0011	
8c ADDRESS (City, State, and ZIP Code) 1400 Wilson Blvd. Arlington, Virginia 22209-2308			10 SOURCE OF FUNDING NUMBERS		
			PROGRAM ELEMENT NO 61101E	PROJECT NO 7A10	TASK NO DA
			WORK UNIT ACCESSION NO CU		
11 TITLE (Include Security Classification) Measurements of High Frequency Seismic Waves					
12 PERSONAL AUTHOR(S) William H. Menke					
13a TYPE OF REPORT Final		13b. TIME COVERED FROM 3/16/87 TO 3/13/89		14 DATE OF REPORT (Year, Month, Day) 1989 December 4	
15. PAGE COUNT 52					
16 SUPPLEMENTARY NOTATION <i>delta</i> <i>1/km</i> <i>1/Hz</i> <i>delta</i>					
17 COSATI CODES			18. SUBJECT TERMS (Continue on reverse if necessary and identify by block number)		
FIELD	GROUP	SUB-GROUP	Measurements of High Frequency Seismic Waves		
19 ABSTRACT (Continue on reverse if necessary and identify by block number)					
<p>Except for its very onset, the P wave of earthquakes and chemical explosions observed at two narrow-aperture arrays on hard rock sites in the Adirondack Mountains have a nearly random polarization. The amount of energy on the vertical, radial and transverse components is about equal over the frequency range 5-80 Hz, for the entire seismogram. The spatial coherence of the seismograms is approximately $\exp(-cf\Delta x)$, where c is in the range 0.4 to 0.7 km \cdot Hz$^{-1}$, f is frequency and Δx is the distance between array elements. The spatial coherence is approximately independent of component, epicentral azimuth and range, and whether P or S wave coda is being considered, at least for propagation distances between 5 and 170 km. These results imply a strongly and three-dimensionally heterogeneous crust, with near-receiver scattering in the uppermost crust controlling the coherence properties of the waves.</p> <p style="text-align: right;">(1,2) ←</p>					
20 DISTRIBUTION/AVAILABILITY OF ABSTRACT <input checked="" type="checkbox"/> UNCLASSIFIED/UNLIMITED <input type="checkbox"/> SAME AS RPT <input type="checkbox"/> DTIC USERS			21 ABSTRACT SECURITY CLASSIFICATION		
22a NAME OF RESPONSIBLE INDIVIDUAL James Lewkowicz			22b. TELEPHONE (Include Area Code) (617) 377-3222		22c. OFFICE SYMBOL GL/LWH

TABLE OF CONTENTS

Report Documentation Page	i
Summary.....	iv
Task Objectives and Technical Problem.....	iv
General Methodology	iv
Technical Results and Important Findings and Conclusions	iv
Significant Hardware Developments	iv
Special Comments and Implications for Further Research.....	v
Bibliography.....	v
Polarization and Coherence of 5-30 Hz Seismic Wavefields at a Hard Rock Site and their Relevance to Velocity Heterogeneities in the Crust	1
Abstract	1
Introduction.....	2
Site and Instrument Characteristics	2
Polarization	3
Spatial Coherence.....	4
Summary.....	9
References	11
Figure Captions	12
Figures	16



Accession For	
NTIS GRA&I	<input checked="" type="checkbox"/>
DTIC TAB	<input type="checkbox"/>
Unannounced	<input type="checkbox"/>
Justification	
By	
Distribution/	
Availability Codes	
Dist	Avail and/or Special
A-1	

Summary

Task Objectives and Technical Problem:

1. To make high quality array measurements of high-frequency (2-50 Hz) seismic waves generated by natural and artificial sources in ghgh-Q regions.
2. To measure fundamental properties of the seismic wave field, including the polarization and spatial coherence.
3. To infer the scattering and attenuative properties of the earth's crust from measurements of the wave field.

General Methodology:

Several well-calibrated differential arrays were installed in quiet, hard rock sites in NE United States, including the Adirondack mountains and Hudson Valley. The instrumentation included twenty EDA Associate seismic recorders, which are 12 bit gain ranged 3 channel recorders with a sampling rate of up to 200 Hz. Each recorder was connected to a three-component Mark Products L22D geophone, which has a velocity response that is flat between 2 and 50 Hz. We calibrated each of the geophones with a mass-drop test. Timing was accomplished by synchronizing the internal clocks of the recorders to GOES satellite time. The instruments were configured into linear arrays, with a inter-element spacing of between 6 and 200 meters. Four linear arrays were run during this project: ECO1 (a six element array in Newcomb, NY with 15 meter spacing), ECO2 (a six element array in Newcomb, NY with 100 meter spacing), DBM (an eight element array at Dunn Bar Mt., New York with a 6-200 meter spacing) and HUDRISE (a 20 element array near New Paltz, NY, with 1 km spacing). Operation times varied from a few days to six months. These arrays recorded a variety of signals, including small regional earthquakes in New England and Canada, quarry blasts, and shots of the NYNEX and HUDRISE experiment.

The data collected by these arrays were analyzed on a Sun 3/260 computer workstation, and measurements of frequency-dependent polarization and frequency-dependent spatial coherence were made using standard algorithms.

Technical Results and Important Findings and Conclusions:

1. The spatial coherence of the wavefield in these hard-rock sites was determined to be very small, only one sixth to one-half of a wavelength. Very strong scattering occurring near the arrays, even though they were chosen to be in a site that was superficially fairly 'homogeneous'. The coherence decreases smoothly with inter-receiver offset, indicating that we are measuring a robust property of the wavefield, and not simply an instrument coupling problem or outcrop-scale effect. Coherence depends most strongly upon the product of inter-receiver offset and frequency, and is not a measurable function of wave type (that is, P or S) or source-receiver range. This result may imply that the scattering is a self-similar process.
2. The polarization of the onset of the P wave is generally linear, with a direction consistent with the source-receiver geometry over a wide frequency band (at least 5 to 30 Hz). The Polarization of the P wave coda is generally chaotic, with significant tangential motion and a direction that varies strongly with frequency.

Significant Hardware Developments:

We are in the process of building a semi-portable broad-band array, based on Guralp CMG-4 geophones (with a response from 0.02 to 50 Hz), to compliment our high frequency array.

Special Comments and Implications for Further Research:

1. The wavefield (including coda) is coherent over distances large enough that array techniques can be used to improve the signal/noise ratio of measurements.
2. Our modeling of the very small coherence lengths (generally less than one half of a wavelength), indicate that very strong scattering is occurring in the upper kilometer of crust. We can not make direct measurements of processes occurring below that depth, since they are masked by the near-surface scattering. Nevertheless, the fact that the seismograms contain distinct P and S waves indicates that the scattering cannot be so strong that wave field becomes diffusive. We therefore feel that the scattering must be less deep in the earth, with the near-surface scattering possibly representing a heterogeneous weathered zone at the top of the crust. This conclusion needs to be checked by measurements made in boreholes up to 1-2 kilometers deep.
3. Many measurements of shear wave splitting have been interpreted as being due to anisotropy. Typically, the first arriving shear energy is found to be linearly polarized (with a direction that is independent of source location). This shear wave is interpreted as the fast anisotropic shear wave. The time when the polarization becomes non-linear is taken to be the arrival of the slow shear wave, with the time difference being proportional to the amount of anisotropy. Our results suggest that onset of non-linear polarization may in many cases be due to scattering, not to the arrival of a slow shear wave. In these cases, at best a minimum estimate of the amount of anisotropy can be measured. The presence of scattering should be tested for by examining the polarization of the P wave. If it has significant tangential motion, and a polarization that shifts rapidly from linear to non-linear, then a similar behavior of the shear wave should be ascribed to scattering, not anisotropy.

Bibliography:

Menke, W., A.L. Lerner-Lam, and B. Dubendorff, Polarization and Coherence of 5-30 Hz Seismic Wavefields at a Hard Rock Site and their Relevance to Velocity Heterogeneities in the Crust, submitted to Bull. Seism. Soc. Am., 1989.

.

.

.

.

Polarization and Coherence of 5-30 Hz Seismic Wavefields at a Hard Rock Site and their Relevance to Velocity Heterogeneities in the Crust

William Menke^{1,2}, Arthur L. Lerner-Lam¹, Bruce Dubendorff³, and Javier Pacheco^{1,2}

revised for BSSA, November 1989

¹Lamont-Doherty Geological Observatory, Palisades, NY

²Department of Geological Sciences, Columbia University, New York, NY

³Department of Physics, University of Dallas, Irvington, TX

Abstract. Except for its very onset, the P wave of earthquakes and chemical explosions observed at two narrow-aperture arrays on hard rock sites in the Adirondack Mountains have a nearly random polarization. The amount of energy on the vertical, radial and transverse components is about equal over the frequency range 5-30 Hz, for the entire seismogram. The spatial coherence of the seismograms is approximately $\exp(-cf\Delta x)$, where c is in the range 0.4 to 0.7 $\text{km}^{-1}\text{Hz}^{-1}$, f is frequency and Δx is the distance between array elements. Vertical, radial, and transverse components were quite coherent over the aperture of the array, indicating that the transverse motion of the compressional wave is a property of relatively large (10^6 m^3) volumes of rock, and not just an anomaly caused by a malfunctioning instrument, poor instrument-rock coupling, or outcrop-scale effects. The spatial coherence is approximately independent of component, epicentral azimuth and range, and whether P or S wave coda is being considered, at least for propagation distances between 5 and 170 km. These results imply a strongly and three-dimensionally heterogeneous crust, with near-receiver scattering in the uppermost crust controlling the coherence properties of the waves.

Introduction

Seismograms of local and regional events are very complicated at frequencies greater than a few Hz. Distinct seismic phases, such as P, PP, S, SS, etc., are seldom present. Instead, the first arrival is immediately followed by a very complex P wave coda, and the S arrival consists of a sudden increase in amplitude followed by slowly decaying S wave coda. Seismograms from the high-Q regions of north-eastern United States are particularly complicated in this respect, presumably because intrinsic attenuation losses are small and the seismic energy may interact with scatterers in the crust and lithosphere.

We present an evaluation of two properties of the seismograms, polarization and spatial coherence, which measure different aspects of the complexity of the seismograms and the underlying scattering process. These measurements are made with two quasi-linear and narrow aperture arrays with very small interstation spacings - from 7 to 734 m. For comparison, one wavelength of a compressional waves in a medium with a nominal 6.0 km/s velocity is 1200 m at 5 Hz and 120 m at 50 Hz. Our aim is to use these measurements to make inferences about the nature of the heterogeneities that produce the complicated coda. Of particular interest are 1) whether fine-scale horizontal stratification such as that proposed by Sereno and Orcutt [1987] to explain oceanic P_0 coda can satisfy coda properties observed for continental paths or whether laterally varying media are required; 2) whether the distortion of the wavefield indicates weak or strong scattering, and; 3) the spatial distribution of scatterers if they exist.

Site and Instrument Characteristics

The seismograms were recorded by two linear arrays:

1) The ECO array, a six-element linear seismic array operated in State University of New York at Syracuse's Huntington Forest Ecological Center, Newcomb, NY. This is an area of Proterozoic metamorphic bedrock (mostly gneiss and marble) in the south-central Adirondack uplift, covered in places by a thin (0-5 m) layer of glacial till. The array was aligned east-west in a grassy meadow near the south-west corner of Rich Lake, with all sensors cemented to exposed gneiss outcrops. The array aperture was 75 m, with a nominal element spacing of 15 m; and

2) The DBM array, a seven element linear array on the southern flank of Dun Brook Mountain about 11 km southwest of ECO. This is also an area of till-draped Proterozoic metamorphic bedrock. The array had a near-logarithmic interstation spacing from 7 to 354 m giving a total aperture of 734 m, and was oriented northeast-southwest. The seismometers were cemented to glacially-polished outcrops of basal gneisses showing little evidence of weathering.

Each array element consists of a three-component Mark Products, Inc. Model 1.22-D geophone mounted in a pressure-sealed aluminum case. These geophones are passive electromagnetic velocity sensors with a natural period of 0.5 s. The velocity response of each component was determined by a mass-drop test (Figure 1), and is very flat above 3 Hz. Gain level determined from the calibrations have been applied to the seismic recordings. The output of each array element was independently recorded by a EDA Associates Model PRS-4 3-channel digital recorder, with each channel sampled at either 100 or 200 samples/s. The data are gain-ranged, with each sample consisting of sign bit, 12 bit mantissa, and 3 bit gain, giving a total dynamic range of 120 dB.

In this paper we concentrate upon four earthquakes (labeled 1 through 4, Figure 2) recorded by the ECO array that are well distributed in epicentral range (5, 40, 140, 170 km, respectively) and a refraction profile (the New York-New England Experiment, see Luetgert et al., 1989) recorded by the DBM array (Figure 3). The EVO events have good signal to noise ratios in the 3-30 Hz range (Figure 4), so we limit our discussion to that band. The corresponding band at DBM is from 5-25 Hz.

Polarization

If the earth were vertically stratified, then all energy arriving between the P and S waves (which we call the 'P wave coda') would necessarily be polarized in the vertical plane containing source and receiver. The degree to which the P wave coda is polarized outside of this plane is a rough measure of the strength of lateral heterogeneities along the propagation path. We therefore rotated the three-component seismograms into a vertical-radial-tangential (z, r, t) coordinate system, where the radial direction is the horizontal direction in this plane and the tangential direction is normal to it. The rotation angle was alternatively set to that specified by the great circle connecting epicenter and receiver, or by the angle that minimized the first cycle of the tangential component of the P wave. Both these methods give rotation angles within 10° of each other.

While the very first arrival was always polarized in the vertical plane, the amplitude of the P wave coda on the tangential coda always rose to approximately equal the radial amplitude within 1-10 cycles (0.1-0.5 s, Figures 5, 6). All three components were quite coherent over the aperture of the array (with coherence distances of about 100 m at 20 Hz, as we will demonstrate below), indicating that the tangential motion is a property of relatively large ($>10^6 \text{ m}^3$) volumes of rock, and not just an anomaly caused by a malfunctioning instrument, poor instrument-rock coupling, or outcrop-scale effects.

Frequency-dependent polarization analysis, based on the technique developed by Park et al. (1987), was applied to both the very onset of the P wave and the P wave coda (Figure 7). The polarization angle determined by this method for the P wave onset

generally agrees with the great-circle angle over the 5-30 Hz range to within $\pm 15^\circ$ (Figure 8), with the variation across the array for any one event being smaller, about $\pm 7^\circ$. There is a systematic, range dependent azimuth anomaly with a magnitude of about 10 degrees, perhaps due to the deflection of rays from the great circle by large-scale velocity heterogeneities in the crust. The polarization of P wave coda is very complicated, displaying neither linear nor planar polarization. Indeed, we are unable to find a statistical test that can distinguish its polarization from that of random time series with similar spectra. The apparent azimuth and angle of incidence generally vary strongly with frequency, with excursions in excess of 60° from the expected values being common. Nevertheless, this pattern of variation of azimuth and angle of incidence with frequency is reasonably coherent across the entire width of the array (not shown), indicating that it is not primarily an outcrop-scale effect.

The onset of the P wave coda is a superposition of waves scattered by compressional to compressional, compressional to shear, and shear to compressional interactions (and possibly multiple scattering). The shear to compressional interactions must occur close to the source, because of the slow speed of the shear wave. They arrive at the receiver along a path similar to the direct P wave and make only a small contribution to the transverse P wave coda. Similarly, compressional to compressional interactions that occur far from the receiver also have little transverse motion. Compressional to shear wave interactions can have large transverse motion, but the slow speed of the shear wave limits these to the neighborhood of the receiver. The very rapid increase in the ratio of tangential to radial P wave coda energy from zero to about unity over a wide frequency bandwidth (Figures 9, 10) indicates that compressional to compressional and compressional to shear wave scattering near the receiver is of major importance. The ratio near unity may also indicate that multiple scattering is occurring, since Sato's (1984) models of coda envelopes in a weakly scattering medium give much smaller ratios. On the other hand, the clearly defined S wave arrivals observed in the earthquake seismograms indicate that the heterogeneity is not so strong that the diffusive limit of strong scattering has been reached (as has been explored by Dainty and Toksoz (1975) for lunar seismograms).

Spatial Coherence

The coherence between two time series measures the similarity of their shapes in a given frequency band, ranging between zero when they are completely dissimilar and one when they are identical. The coherence between two seismograms $s(x_1, t)$ and $s(x_2, t)$ recorded at positions x_1 and x_2 is typically defined as:

$$C(f, \Delta f, \Delta x) = \frac{|\langle s^*(x_1, f) s(x_2, f) \rangle|^2}{\langle s^*(x_1, f) s(x_1, f) \rangle \langle s^*(x_2, f) s(x_2, f) \rangle} \quad (1)$$

Here $s(x_1, f)$ is the Fourier transform of $s(x_1, t)$ over frequency, f , $\langle \rangle$ denotes boxcar averaging over a frequency interval Δf centered on f , $*$ denotes complex conjugation, and we have assumed that coherence is stationary in that it depends on relative receiver separation $\Delta x = x_1 - x_2$. As it stands, this definition of coherence is unsuitable for our analysis, because it does not account for the possibility of different levels of coherence between different time intervals in the signals (the P and S waves, for example), and does not account for any moveout between the signals caused by propagation between stations. We therefore adopt a moving-window coherence in which the two signals are divided into several smaller sections and corresponding sections of the two signals are allowed to be lagged with respect to each other. The new signal is, $S(x_i, t) = W(t_0, \Delta T) s(x_i, t)$, where $W(t_0, \Delta T)$ is a cosine-tapered window function centered on time, t_0 , and of length, ΔT and sampling interval, Δt . The coherence is then defined as:

$$C(f, \Delta f, \Delta x, t_0, \Delta T, \epsilon) = \max_{\tau} \frac{|\langle S^*(x_1, f) e^{2\pi i f \tau} S(x_2, f) \rangle|^2}{\langle S^*(x_1, f) S(x_1, f) \rangle \langle S^*(x_2, f) S(x_2, f) \rangle} \quad (2)$$

$|\tau|/\Delta t \leq \epsilon$

The factor of $\exp(2\pi i f \tau)$ has the effect of allowing for small time shifts between the two signals. In this paper, we use $\Delta f = 5$ or 6 Hz, $\Delta T = 0.5$ – 2.6 s, and $\epsilon = 20$. Successive windows are lagged by $\Delta T/2$, giving some overlap and effective smoothing of the moving-window calculation.

The maximization of the coherence with respect to lag causes some upward bias in the coherence estimate, even for completely random, incoherent timeseries. This is because the process of lagging the signals will tend to align random similarities that may be present. We have investigated this effect by Monte-Carlo simulation, and have found that it changes the coherence by less than 0.1 (Figure 11). In all of our calculations, a coherence greater than 0.3 is distinguishable from incoherence at the 95% confidence level.

Finally, we can define a mean coherence, C_m , of a long seismogram as the expected value of the coherence of its many windows. In this paper we use the arithmetic mean as a estimate of the expected value, even though the coherence estimates do not have a gaussian

distribution (being constrained to lie between zero and unity). This approximation causes some bias in the estimate. However, Monte Carlo experiments (Figure 12) using the window lengths and other parameters from our analyses indicate that the bias for our particular estimates are small, less than 0.05 coherence units. C_m is computed for the first 15 s after the P arrival, averaged over epicentral ranges less than 250 km (see Figure 3).

The moving-window coherence for the entire DBM NYNEX record section is shown in Figure 13. Note that the coherence does not vary much with range (the decrease in coherence with time in the S-wave coda is due to the decrease in the signal to noise ratio) and that the wavefield is more coherent at small inter-station offsets than at large ones. The coherence of the vertical, radial, and transverse components of the data can be summarized as follows:

1. The coherence of the P wave onset is usually higher than the rest of the seismogram on both vertical and radial components, by about 10-20% (Figure 14).
2. The coherence of the S wave and its coda is broadly similar to the coherence of the P wave coda (Figures 15 and 17).
3. The coherence of P wave coda is greatest on the vertical component, which tends to be 5-10% more coherent than the radial and transverse components. The coherence of the radial and transverse components are not significantly different (Figure 16).
4. Coherence is independent of epicentral range and azimuth relative to the axis of the array (at least for ranges between 5 and 200 km, Figure 15 and 17), but decreases strongly with both frequency, f , and station separation, Δx (Figure 18). The mean coherence at an array can be fit between 5 and 25 Hz by the empirical function, $C_m = \exp\{-cf\Delta x\}$, where $c=0.41 \text{ km}^{-1} \text{ Hz}^{-1}$ for the ECO array (Figure 18), and where $c = 0.67 \text{ km}^{-1} \text{ Hz}^{-1}$ for the DBM array. We do not claim that the true coherence is necessarily an exponential, just that this formula satisfactorily describes the observed pattern of variation (which, after all, has considerable scatter). Since the compressional velocity in bedrock beneath the array is about 5 km/s, we can also write this formula as $C_m = \exp\{-k \Delta x/\lambda_p\}$, where λ_p is the wavelength of the compressional wave and k is in the range 2-3. The coherence length is on the order of one third to one half a wavelength.

The high coherence of the P wave onset can be understood from the fact that this energy arrives first and cannot have been incoherently scattered by heterogeneities in the earth. The similar pattern of coherence of the three components of P and S coda waves is a strong argument for the importance of multiple scattering. Sufficient number of scattering interactions must have taken place so that the energy is equally distributed between all possible modes of propagation, regardless of its origin. The ratio of compressional to

shear wave energy in the P wave coda must be very similar to that in the S wave coda, because the coherence decreases with inter-station offset at the same rate in both cases, even though the wavelength of compressional waves is about $\sqrt{3}$ larger than the wavelength of shear waves. The characteristic offset, $(\Delta x)_c$, in which the coherence decays to $1/e$ is quite small, about one-third to one-half wavelength.

The dependence of mean coherence on the combination $f\Delta x$ (or $\Delta x/\lambda_p$) and its independence of source-receiver range implies that the only important length scale governing the scattering is the wavelength of the seismic energy (and not the source-receiver distance). One model that fits the data places the scatterers that control the coherence in a layer of thickness, L , near the earth's surface (and the array). No conclusion can be reached about the scatterers elsewhere along the propagation path. The near-receiver scattering is presumed to be sufficiently strong that it 'masks out' scattering from greater distances.

We have performed a simple calculation to crudely model this situation. We assume that the scattering is due to N discrete point sources in a volume, V , beneath the array, all radiating with a white spectrum and randomly chosen phase, ϕ . The point sources model the waves scattered from the heterogeneities in the earth when they are illuminated by some incident wave. The initial phase is chosen randomly, since it will depend upon the strength of the random heterogeneity. The signals observed at two stations, one located at x_1 and the other at $x_2 = x_1 + \Delta x$, are then:

$$s_1(f) = \sum_{j=1}^N |x_1^{(j)}|^{-1} \exp\{2i\pi f c^{-1} \mathbf{n}^{(j)} \cdot \mathbf{x}_1^{(j)} + i\phi\} \quad (3)$$

and

$$s_2(f) = \sum_{j=1}^N |x_2^{(j)}|^{-1} \exp\{2i\pi f c^{-1} \mathbf{n}^{(j)} \cdot \mathbf{x}_2^{(j)} + i\phi\} \quad (4)$$

where $\mathbf{n}^{(j)}$ is a unit vector from the j -th scatterer to the receiver. The ensemble-averaged mean coherence of these two signals (which we compute numerically) roughly matches the observed coherence when $V = 1250 \text{ km}^3$, N is in the range 100-1000, and where the volume extends to the earth's surface. When the scattering volume is moved to a depth of 5 km, the coherence decays with offset too slowly to fit the data (Figure 19). However, the shape

of the model coherence curves differ significantly from the data, being modeled better by $C_m = \exp\{-k(f\Delta x)^2\}$, than by $\exp\{-cf\Delta x\}$. The coefficient, k , of the model is also 40% smaller than that of the data. We attribute these effects to the simplicity of the model, which ignores many effects, including the variation of the initial phase with frequency.

Summary

Although the compressional wave coda has a very complex polarization, the three components of motion have a very high coherence between neighboring stations in both the ECO and DBM arrays. The complex polarization is a robust property of the wavefield, and not merely an outcrop-scale effect.

The major characteristics of the polarization are 1) The onset of P is polarized in the manner expected from the source-receiver orientation; 2) The polarization P and S coda are similar to those of random time series; and 3) The ratio of energy on the transverse component to radial component rapidly rises from zero at the onset of P to about unity in 1-10 cycles, over the 5-30 Hz band.

These results cannot be explained by a vertically stratified model (which has no transverse compressional motion). Travel time considerations suggest that compressional to shear wave scattering near the receiver is occurring. The presence of complex polarization poses problems for experiments designed to measure shear wave splitting due to anisotropy, since the transition from a first-arriving shear wave (where the polarization is linear) to the second-arriving shear wave (where the polarization becomes complex) may be masked by scattering. Measurements of the splitting time may be minimum estimates, with corresponding minimum estimates of the amount of anisotropy. We suggest that the disturbing effect of scattering be tested for by examining the polarization of the compressional wave. Any apparent 'splitting' of the compressional wave implies strong scattering, and makes measurements of shear wave splitting suspect. On the other hand, a linear increase in the splitting times with source-receiver range supports the conclusion that the splitting is indeed due to anisotropy.

The coherence in the 5-30 Hz band decreases smoothly with receiver separation. No instances of sharp drops between stations were observed, as might be caused, say, by the acoustic isolation of parts of the array by joints or faults between the receivers. Of course, the receiver sites in both arrays were carefully chosen to be on what looked like firm bedrock, so the experimental design discriminated against such effects.

The coherence results are: 1) The spatial coherence of the seismograms is approximately $\exp\{-cf\Delta x\}$, where $c=0.4$ to $0.7 \text{ km}^{-1}\text{Hz}^{-1}$, f is frequency and Δx is station offset, at least for the distance range 5-238 km; and 2) The spatial coherence is

approximately independent of component, epicentral azimuth and range, and whether P or S wave coda is being considered.

These results imply that the heterogeneities are three-dimensional and that scattering from near-receiver heterogeneities controls the coherence properties of the seismograms.

Acknowledgements. We thank Klaus Jacob, Bob Busby, and other members for the National Center for Earthquake Engineering Research for providing field support. Ted Koczynski and Dave Lentricchia helped with the instrumentation. We thank the staff of the Huntington Forest Ecological Center for the generous use of their facilities. This research was supported by the Defense Advanced Research Projects Agency under Contract F19628-97-K-0011, the Office of Naval Research under contract N00014-87-K0204 and the National Science Foundation under grants EAR87-96171 and EAR88-1303. Lamont Doherty Contribution 00000.

References

- Dainty, A.M. and M.N. Toksoz, Elastic wave propagation in a highly scattering medium - a diffusive approach, *J. Geophys.* 43, 375-388, 1975.
- Luetgert, J.H., Hughes, S., Forsyth, D., and Cipar, J., The 1988 Ontario-New York-New England seismic refraction experiment: description and early results, *EOS Trans. AGU*, 70, 400, 1989.
- Park, J., F.L. Vernon III and C.R. Lindberg, Frequency-dependent polarization analysis of high-frequency seismograms, *J. Geophys. Res.* 92, 12664-12674, 1987.
- Sato, H., Attenuation and envelope formation of three-component seismograms of small local earthquakes in randomly inhomogeneous lithosphere, *J. Geophys. Res.* 89, 1221-1241, 1984.
- Sereno, T.J. and J.A. Orcutt, Synthetic Pn and Sn phases and the frequency dependence of A of oceanic lithosphere, *J. Geophys. Res.* 92, 3541-3566, 1987.

Figure Captions

Fig. 1. Velocity response for the vertical channel of one of the geophones used in the study. The response of the other elements and channels is similar. Note that the response is very flat between 3 and 30 Hz.

Fig. 2. Vertical-component seismograms for one of the stations of the ECO array for 4 events (labeled 1-4) used in the study. Source-receiver distance are 5, 40, 140 and 172 km.

Fig 3. Record section of the vertical component of one of the elements of DMB array. The shots, part of the New York - New England seismic experiment (NYNEX) organized by the U.S. Geological Survey and Air Force Geophysical Laboratory, were along a roughly east-west line and consisted of about 1000 kg of ANFO explosive in a 30-50 m deep borehole. The shaded part of the seismograms were used in the calculation of coherence, described later in the paper.

Fig. 4. Amplitude spectrum of velocity seismogram of signal (bold) and noise (solid) for a typical event recorded by the ECO array. Note that the signal to noise ratio is high (greater than 10) for the frequency band 3-30 Hz.

Fig. 5. First arrival (marked P) and onset of P coda for four events recorded by the ECO array. Two components, radial (R) and transverse (T) are shown. Note that amplitude of the tangential component is small during the onset, but rapidly rises to roughly equal the amplitude of the radial component.

Fig. 6. The radial (left column) and transverse (right column) components of the P wave coda of event 1 for various choices of the rotation azimuth (measured relative to the great-circle azimuth, so that the lowest traces, labeled zero, are the ones used in the study. Note that the transverse component of the onset of P is smallest only for rotation angles near zero. The rest of the P wave coda cannot be rotated into an optimal radial direction for any choice of angle.

Fig. 7. Frequency-dependent polarization for four time windows in the P wave coda of Event ECO 4. Windows are delimited by vertical bars, with first window shaded.

Azimuth is measured counter-clockwise from geometrical azimuth, angle of incidence from vertical. Note that the azimuth of the first window, which includes the first arriving waves, is within $\pm 5^\circ$ of zero (the geometrical azimuth) for the frequency band 2-20 Hz. The azimuth of subsequent windows is typically $30\text{-}40^\circ$ from the geometrical azimuth and varies strongly with frequency. Six tapers are used in the frequency-dependent polarization analysis.

Figure 8. Polarization anomalies for the onset of P (0.64 s windows) in the New York - Nex England refraction experiment as observed at the DBM array. Data are arranged by increasing station-event range, with the western ranges plotted as negative and the eastern as positive. Data are shown for two frequency bands: 5-10 Hz (circles) and 10-20 Hz (crosses). Six tapers are used in the frequency-dependent polarization analysis. Note that the polarization anomalies are about $\pm 15^\circ$ and that the spread for any given range (which corresponds to a single shot observed by the elements of the array) is smaller, about $\pm 7^\circ$.

Fig. 9. Ratio of transverse to radial component of event 1 for 5 Hz (top graph) and 30 Hz (second graph). The ratio rapidly grows to about unity. These ratios were computed by taking the ratio of the envelopes of the transverse and radial seismograms, where the envelope is the time-averaged sum of the squared signal and the square of its Hilbert transform. The radial (third graph) and tangential (bottom graph) seismograms are shown for reference.

Fig. 10. Ratio of transverse to radial component of event 4 for 5 Hz (top graph) and 30 (second graph) Hz. See caption of Figure 8 for details.

Fig. 11. 95% confidence limits for the null hypothesis that two time series have non-zero coherence, as a function of frequency. The different curves correspond to different time windows ($\epsilon\Delta t$ in equation 2) over which the coherence is maximized. Increasing the time window increases the 95% confidence limit slightly. For the cases described in this paper, coherences greater than 0.3 are statistically significant.

Fig. 12. Mean coherence of a pair of 320 s long time series (not shown), determined by computing the coherence of several windowed portions of the time series and then taking the arithmetic mean of the results. The time series are broad band, random time series with an actual coherence of 0.9. The estimated mean coherences are generally biased to values

lower than 0.9, and vary slightly with the window length. However, the bias is small (less than 0.05), and deemed by us to be acceptable.

Fig. 13. Coherence (1.0-0.8 shaded black, 0.8-0.3 gray, 0.3-0.0 white) as a function of frequency (horizontal axis, from 0 to 50 Hz) and time in the seismogram (vertical axis, from 0-30 s) for the NYNEX refraction shots observed at the DBM array. Source-receiver distance increase from panel to panel horizontally, and inter-receiver offset increase vertically. Note the smaller offsets are the most coherent. Coherences greater than 0.3 are statistically significant.

Fig. 14. Moving-window coherence of radial component of P wave coda of ECO Event 4. Four frequencies are shown: 5 Hz (bold), 10 Hz (solid), 20 Hz (dotted), 30 Hz (dashed). The station offset is 75 m. Note that the coherence of the very onset of P (at about 5s) is higher than the later coda. The overall level of the coherence declines with frequency. Coherences greater than 0.3 are statistically significant.

Fig. 15. Mean coherence (dots) and error bars as a function of frequency for the first 30 seconds following the P wave for the vertical component of the DBM NYNEX dataset. The four curves are for the four receiver offsets, 7, 19, 29, 50 m, with the smaller offsets having the higher coherences. Note that error bars are small, especially in the 5-30 Hz band where the signal to noise ratio is the best, even though the moving-window coherences that are stacked to compute mean coherence are for different ranges (in the interval 10-200 km) and different parts of the seismogram (15 different 2 second windows following the P wave). Coherences greater than 0.3 are statistically significant.

Fig. 16. Moving-window coherence of vertical, radial, and transverse components of P wave coda of ECO Event 1. Four frequencies are shown: 5 Hz (bold), 10 Hz (solid), 20 Hz (dotted), 30 Hz (dashed). The station offset is 75 m. Note that the coherence of the very onset of P (at about 5s) is higher than the later coda. The overall level of the coherence declines with frequency. Coherences greater than 0.3 are statistically significant.

Fig. 17. Mean coherence, C_m , of the P wave coda (solid) and S wave coda (bold) of ECO events 1, 2, 3 and 4 as a function of offset, A_x . Event 1 has a range of 5 km and Event 4 has a range of 172 km. Four frequency bands are shown, 5 Hz, 10 Hz, 20 Hz, 30 Hz. Note that the decay rate of the coherence with offset is insensitive to source range and

whether P or S coda is being considered. Coherences greater than 0.3 are statistically significant.

Fig. 18. (Top) Mean coherence of all data as a function of receiver offset, and exponential fits. Same symbols as Figure 10. (Bottom) Decay rates as determined by exponential fits as a function of frequency (solid), and linear fit (bold). Coherences greater than 0.3 are statistically significant.

Fig. 19. Ensemble-averaged mean coherence (crosses) for the simple scattering model described in the text, and Gaussian fits (solid), for two choices of the depth to the top of the scatterer volume, 100 m (top) and 5 km (bottom). Shallow scatterers fit the observed coherences (Figure 11) better than deep ones.

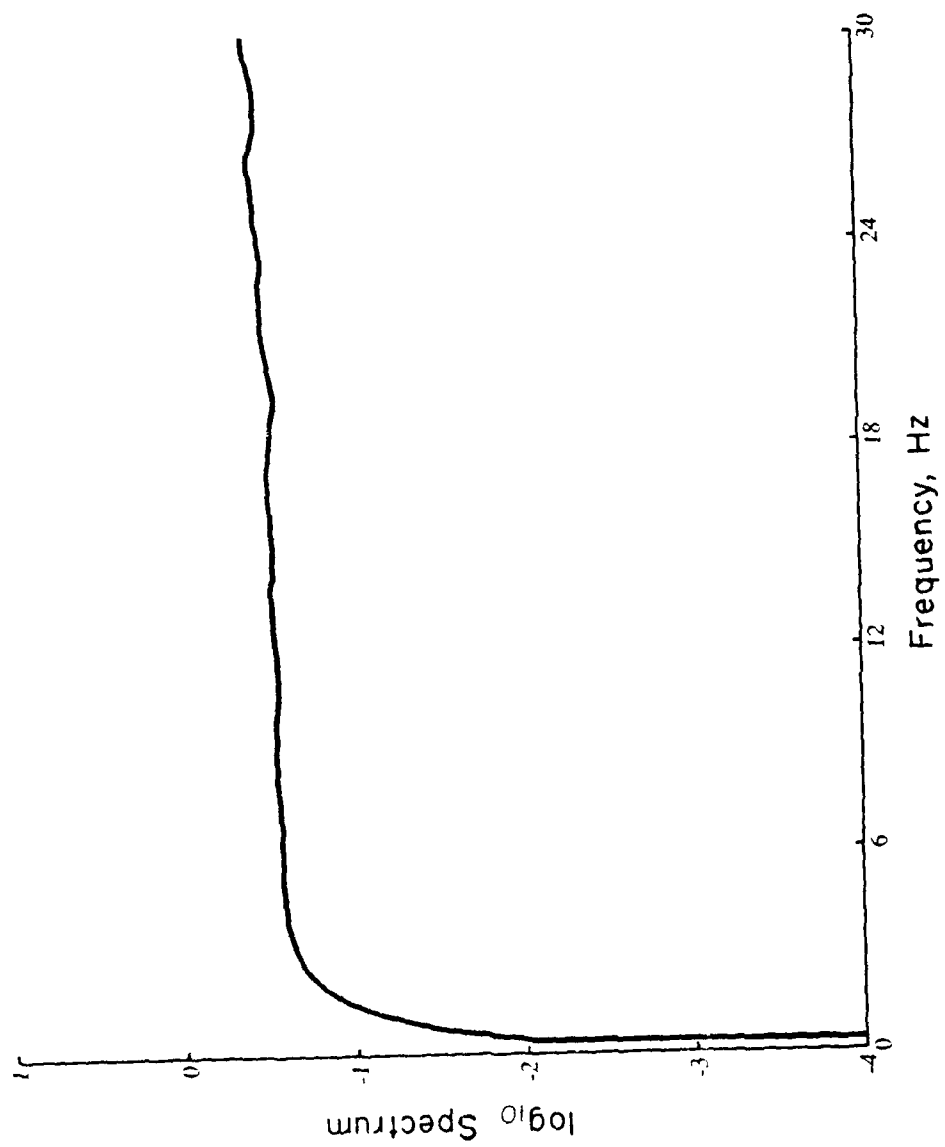


FIGURE 1

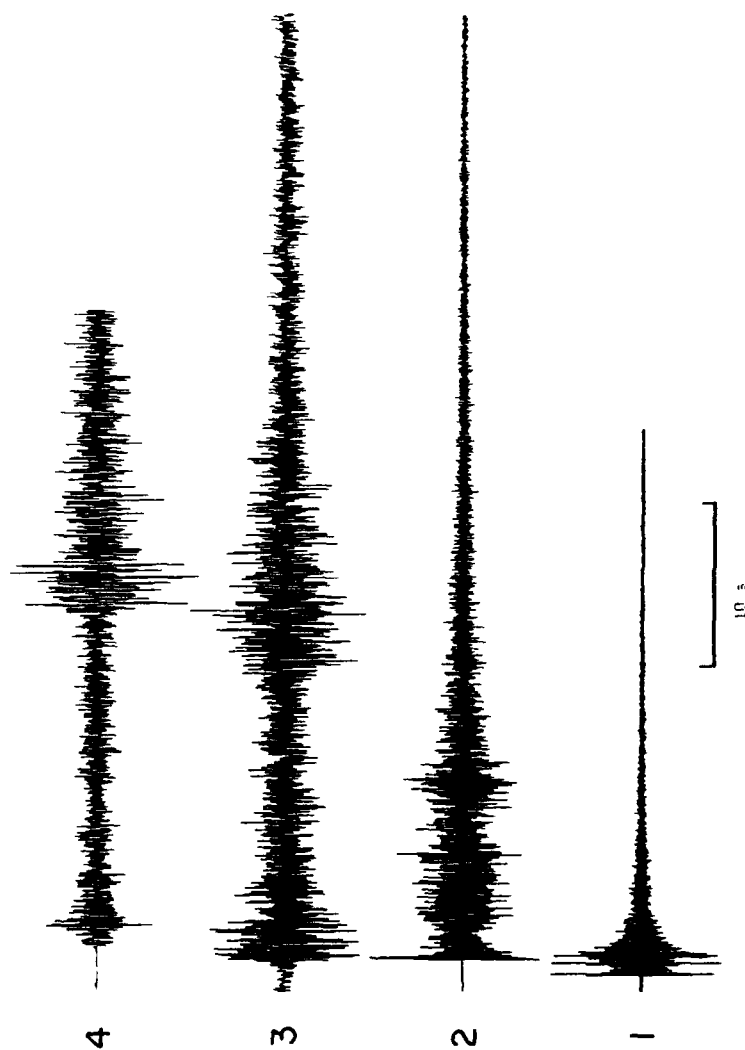


FIGURE 2

DUN BROOK MOUNTAIN ARRAY ELEMENT 2

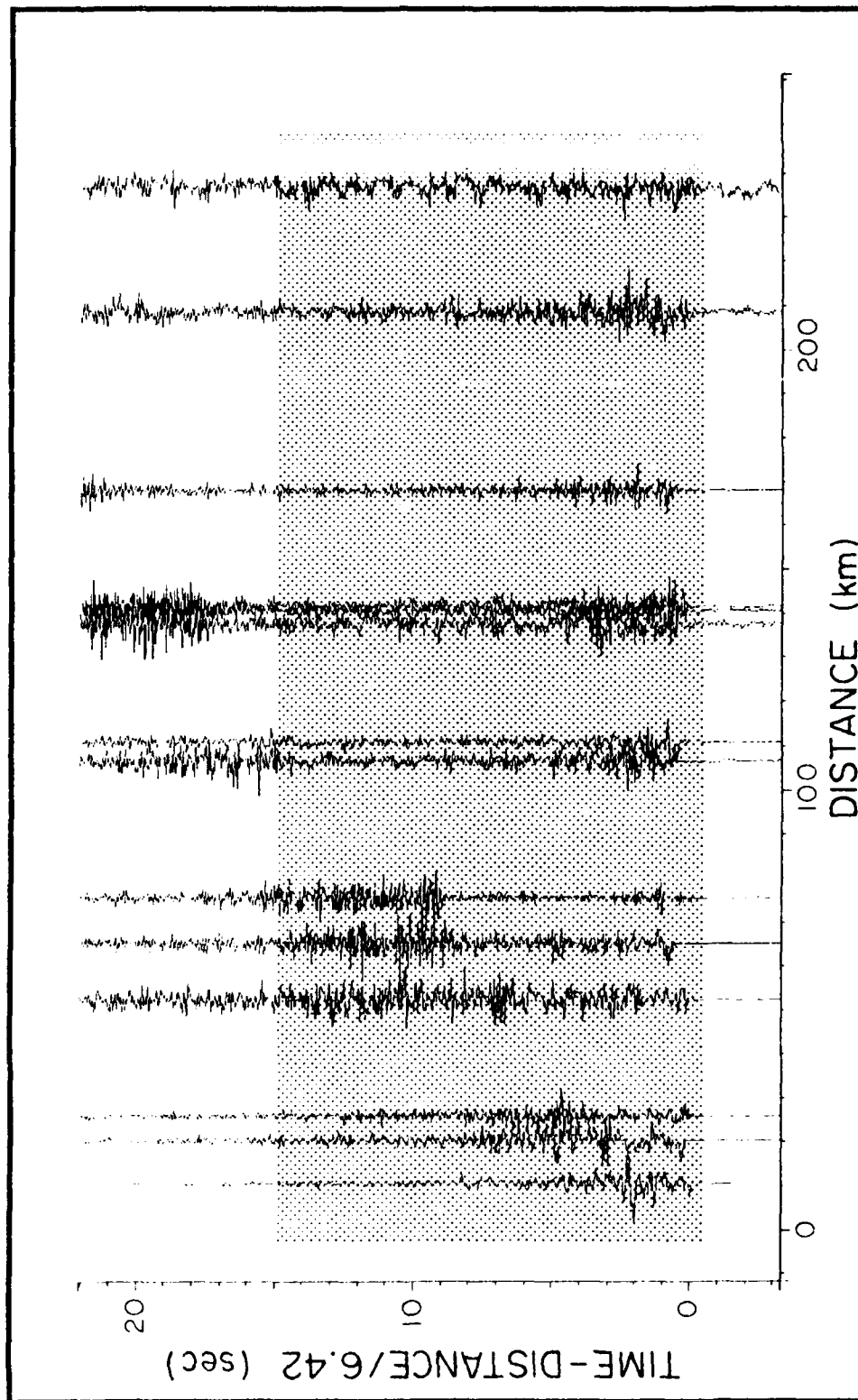


FIGURE 3

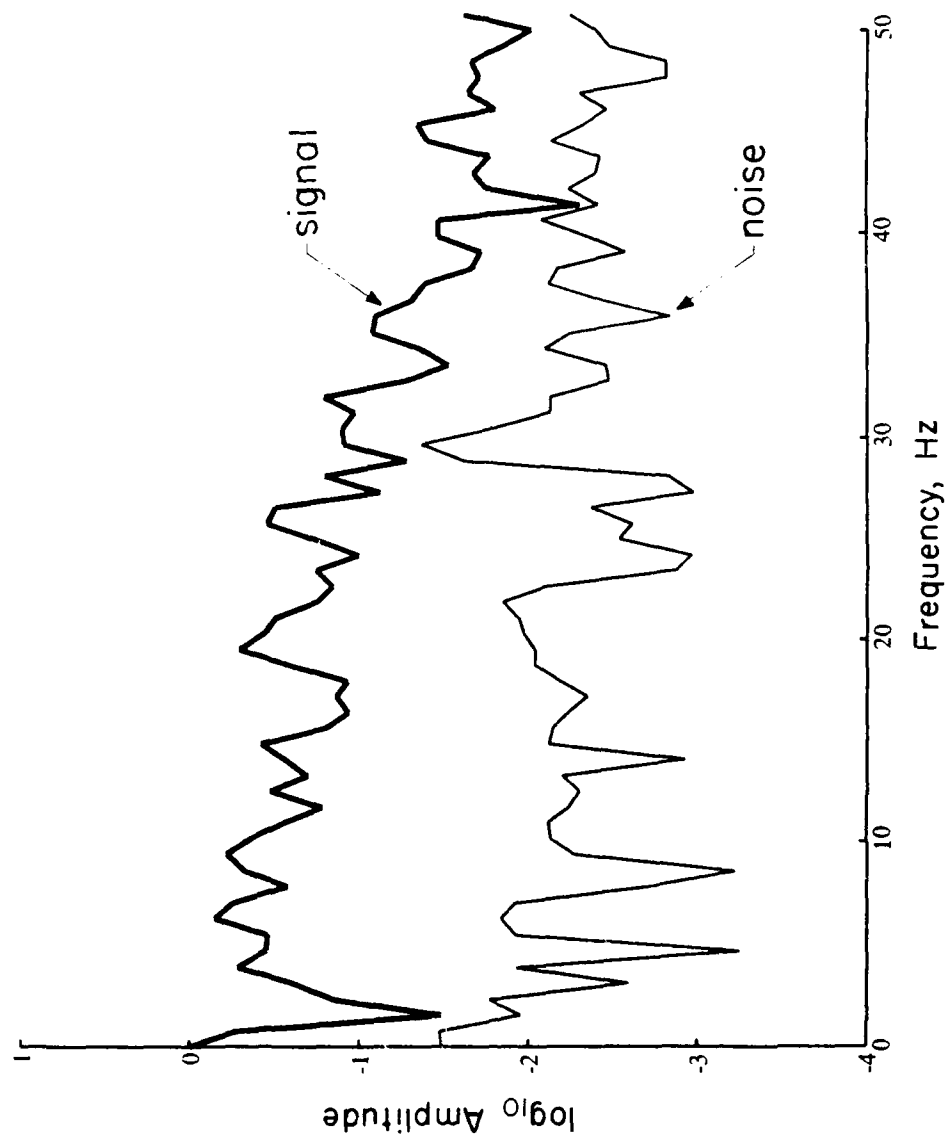


FIGURE 4

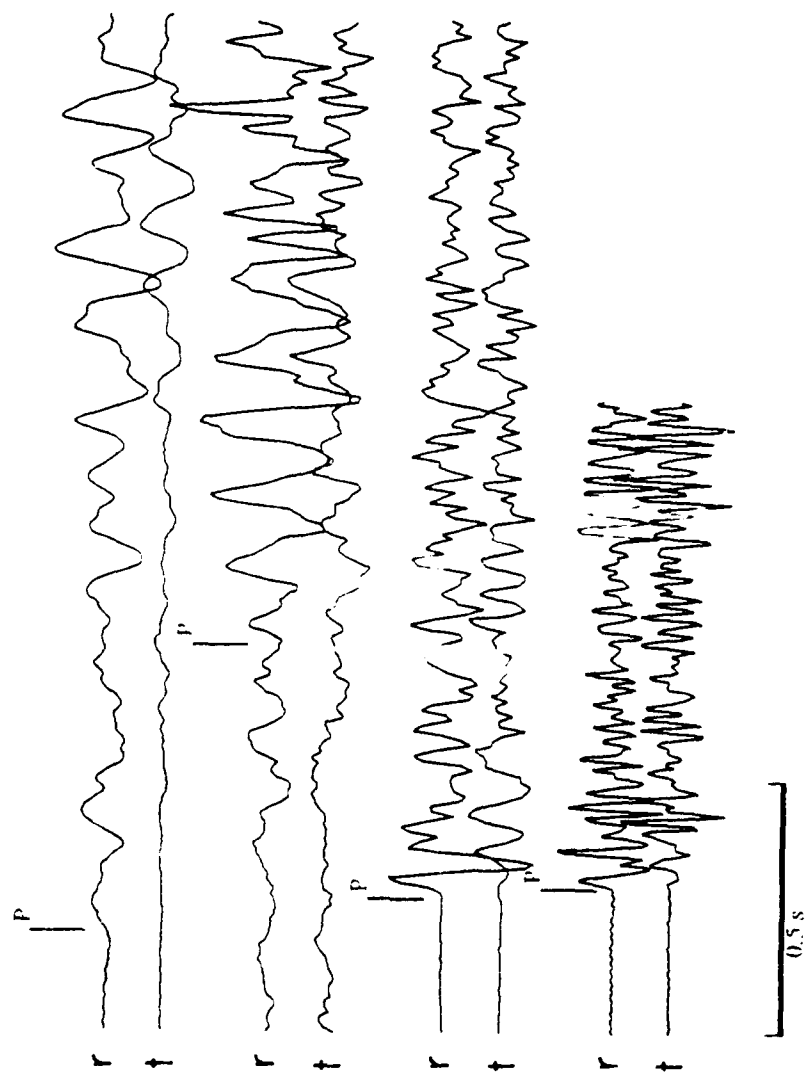


FIGURE 5

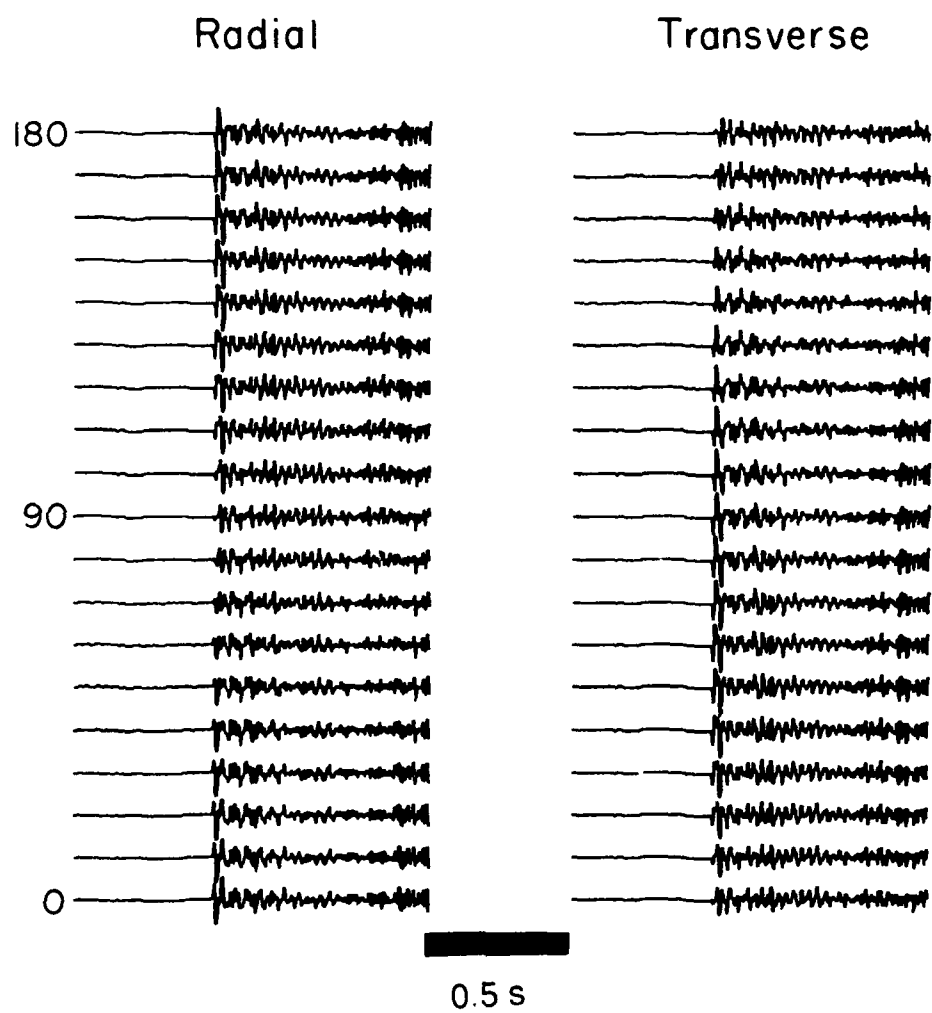
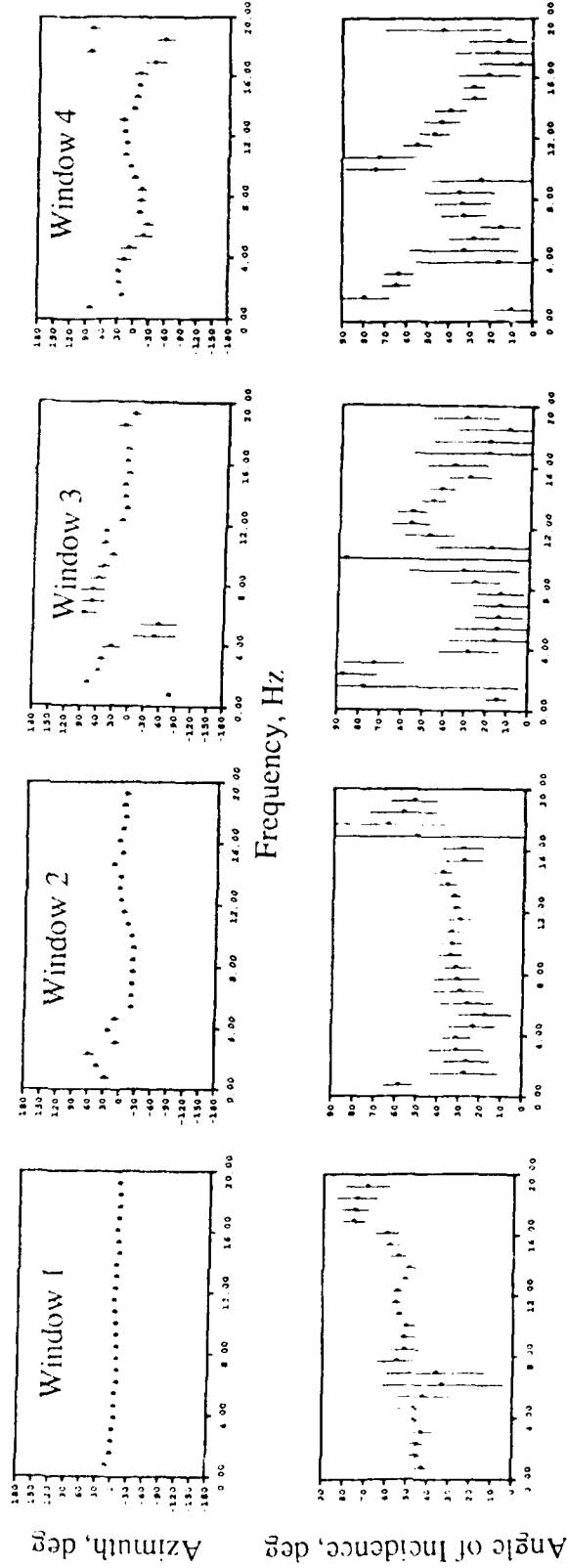
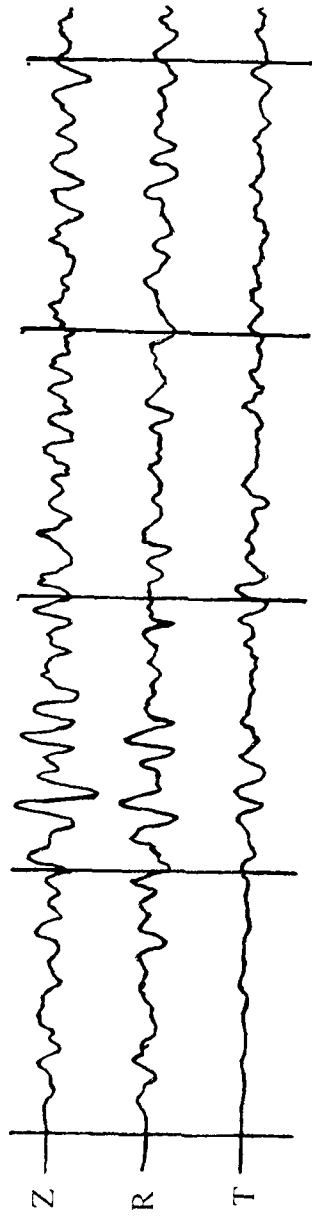


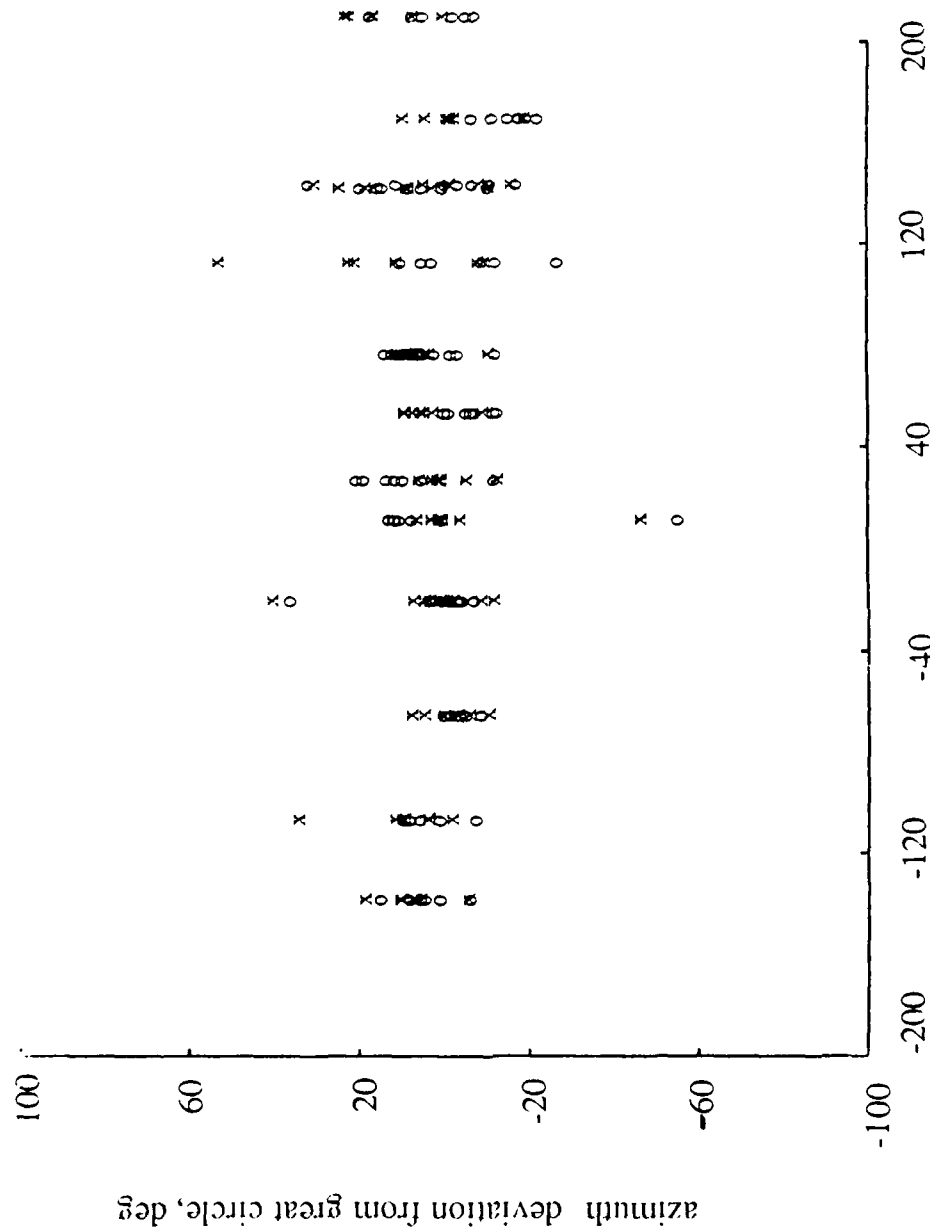
FIGURE 6

ECO EVENT 4



Frequency, Hz

FIGURE 7



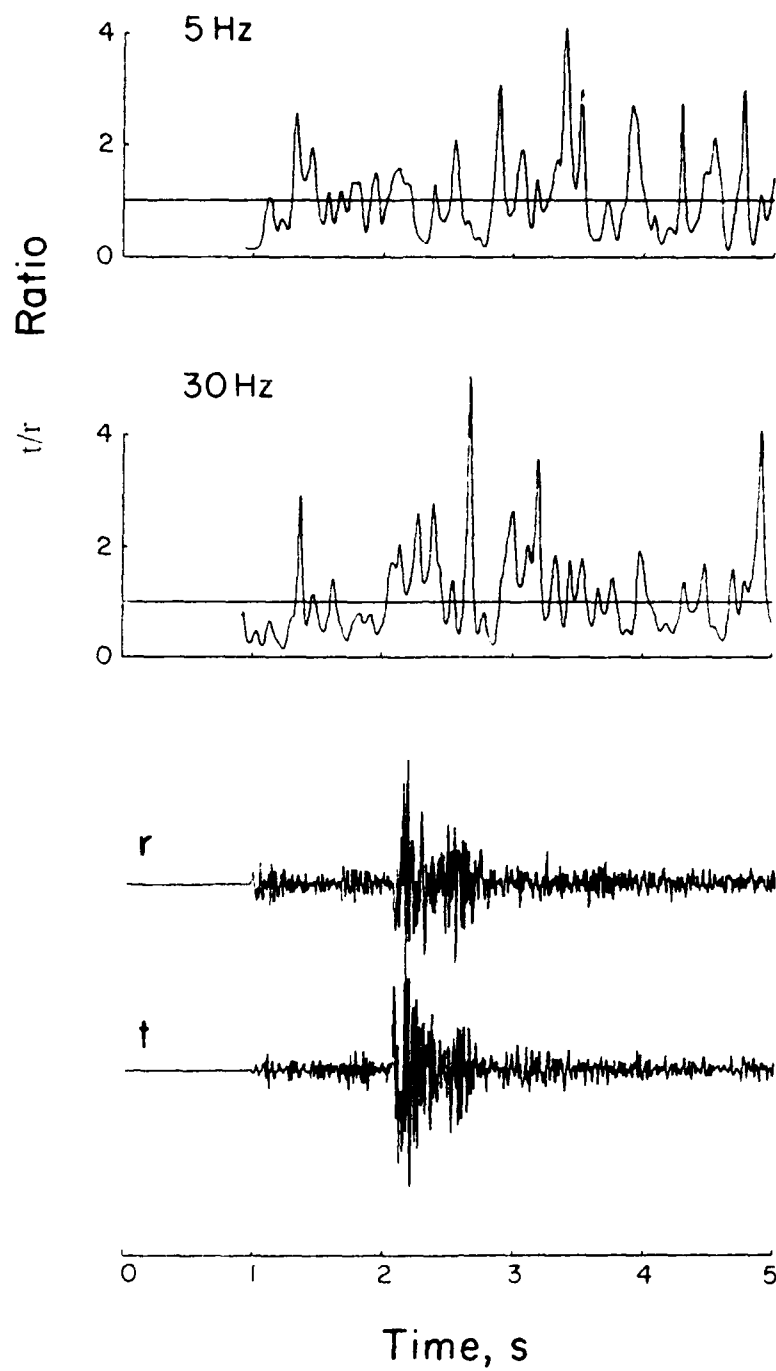


FIGURE 9

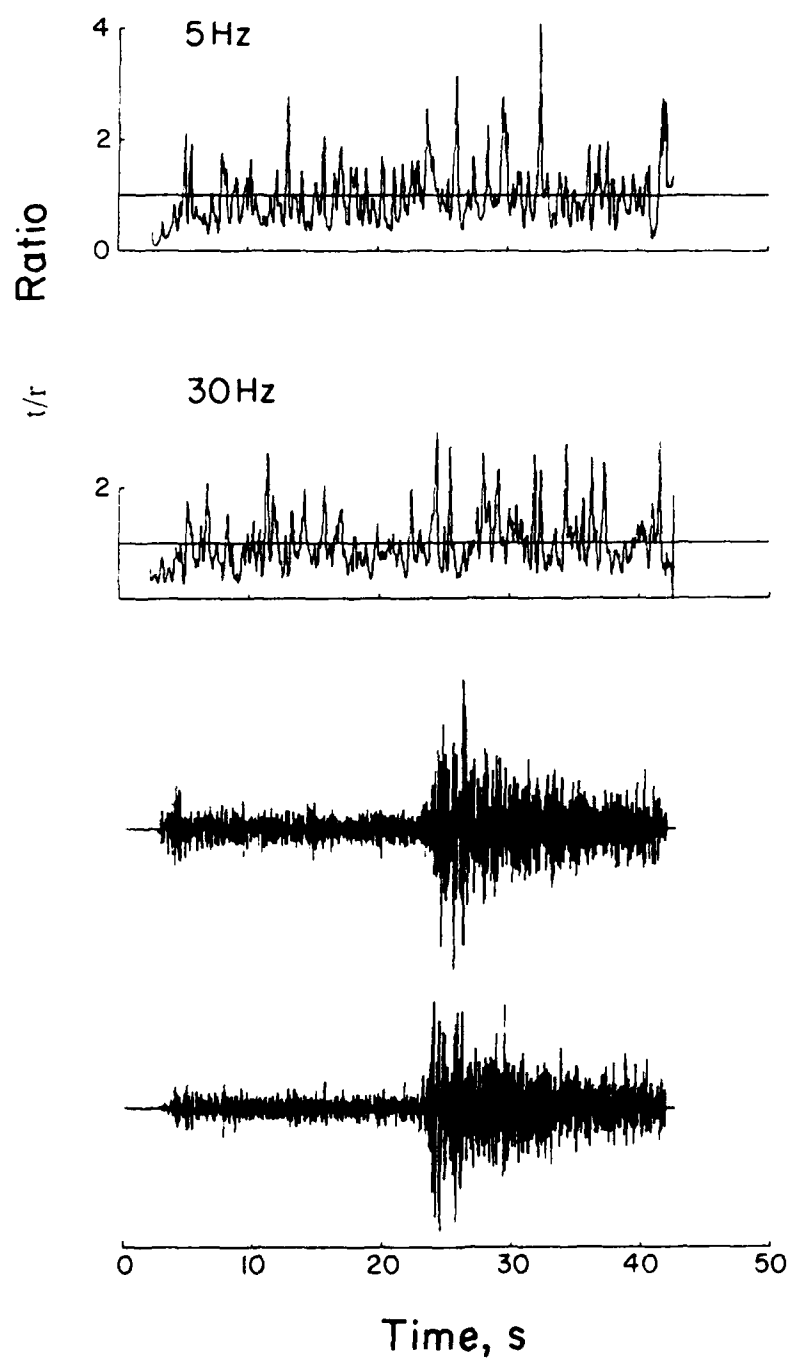


FIGURE 10

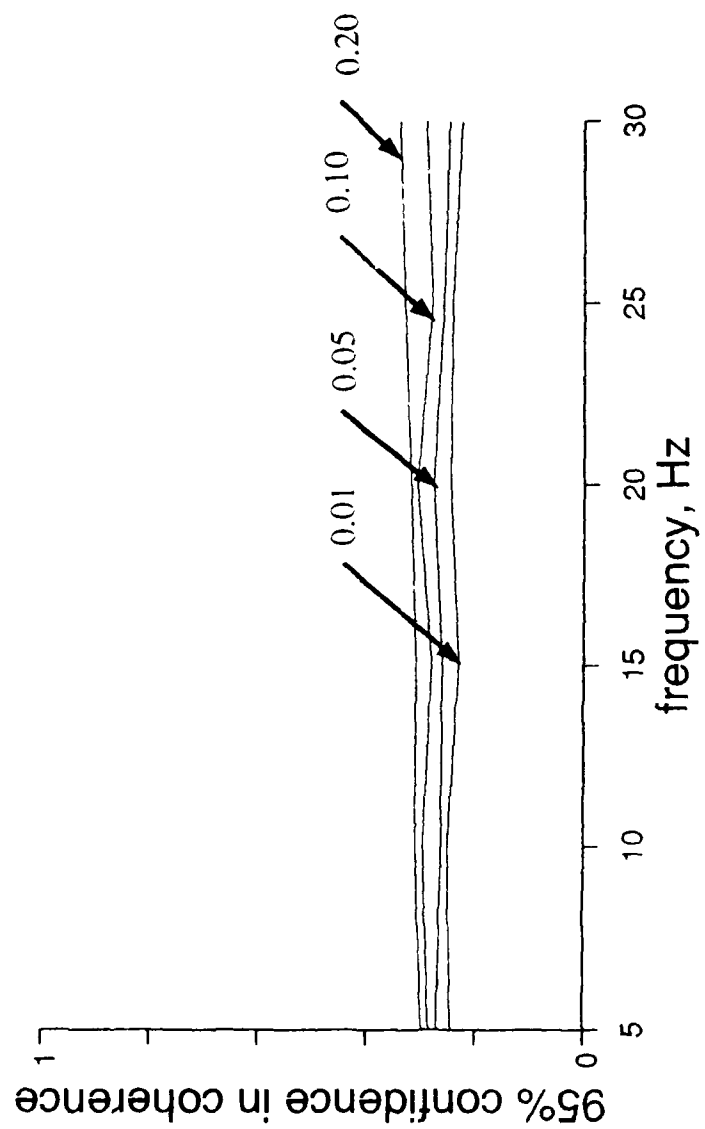


FIGURE 11

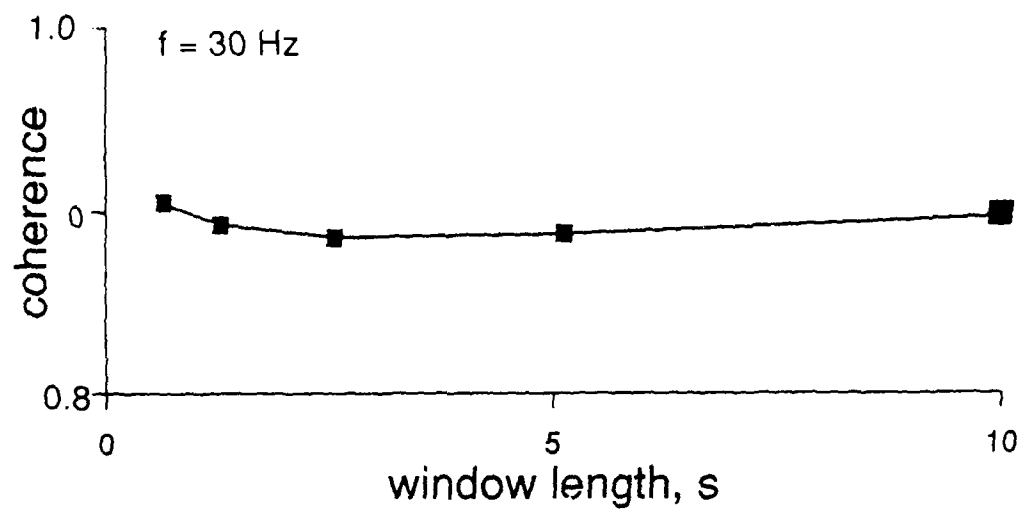
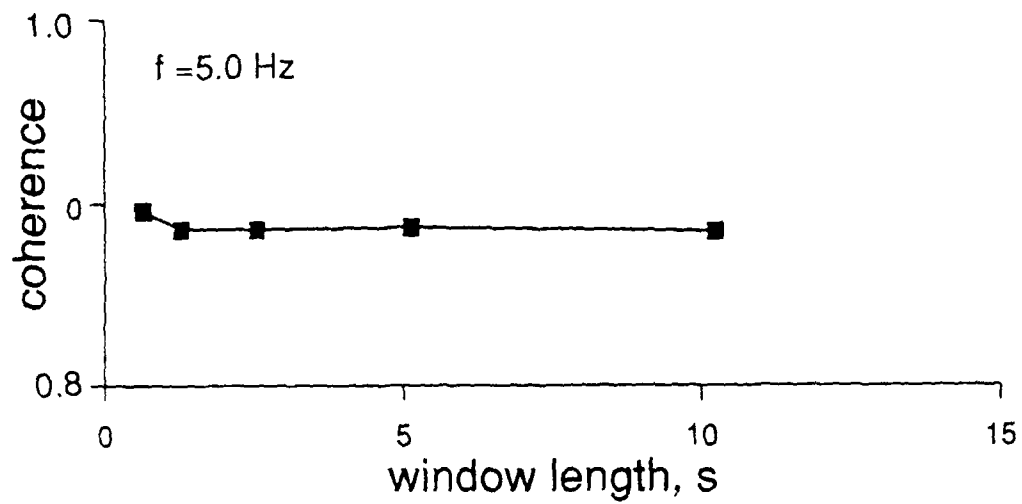


FIGURE 12

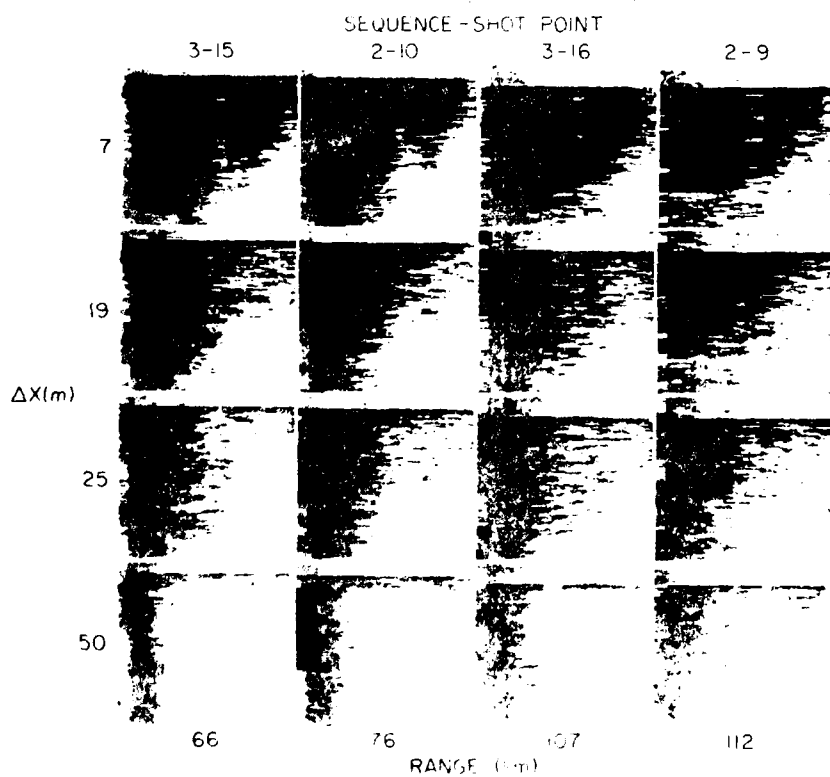
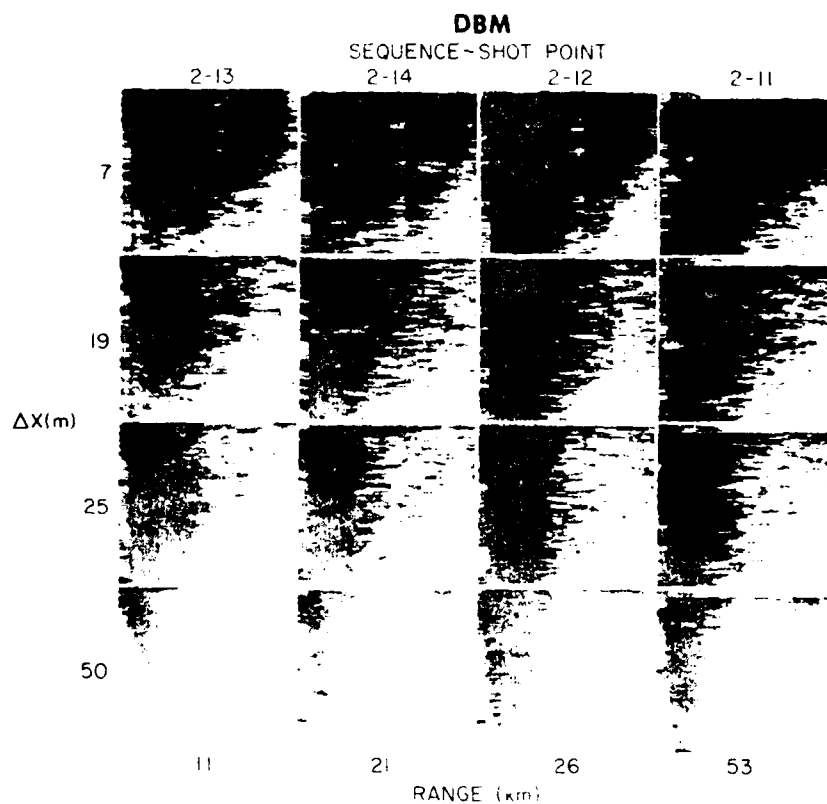


FIGURE 13

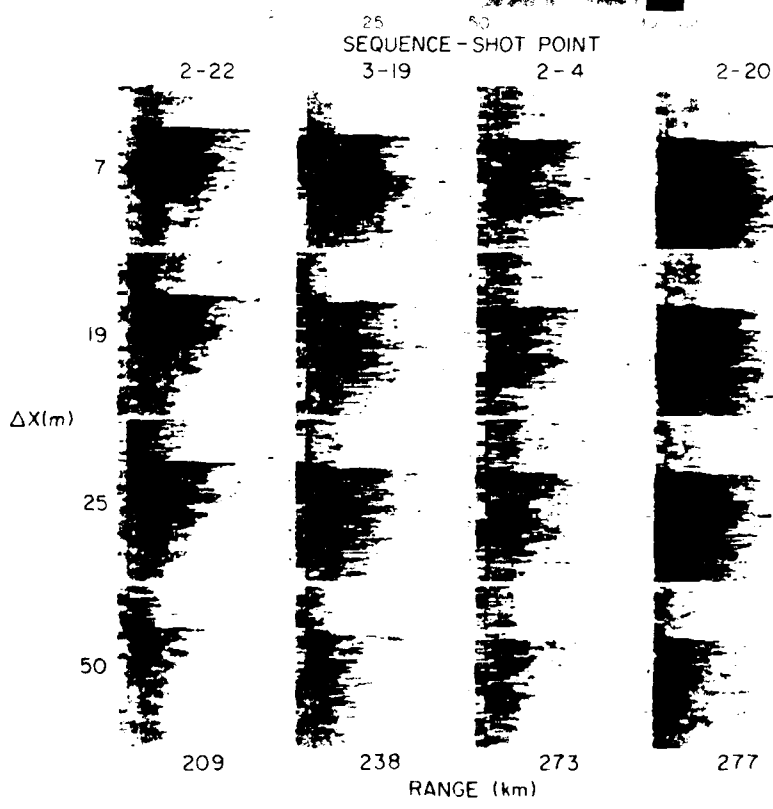
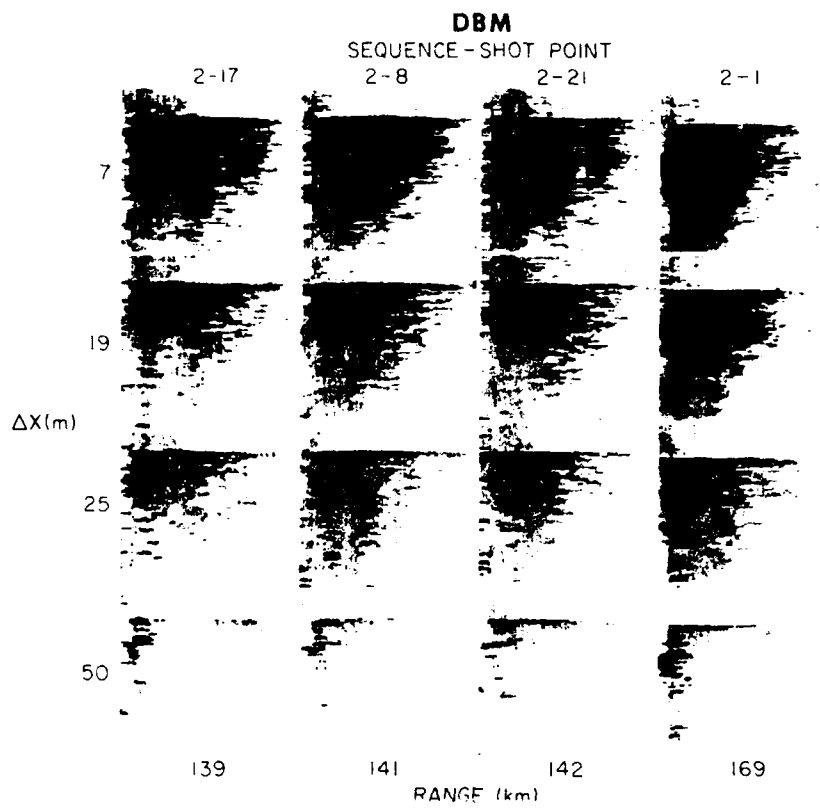


FIGURE 13 (Cont)

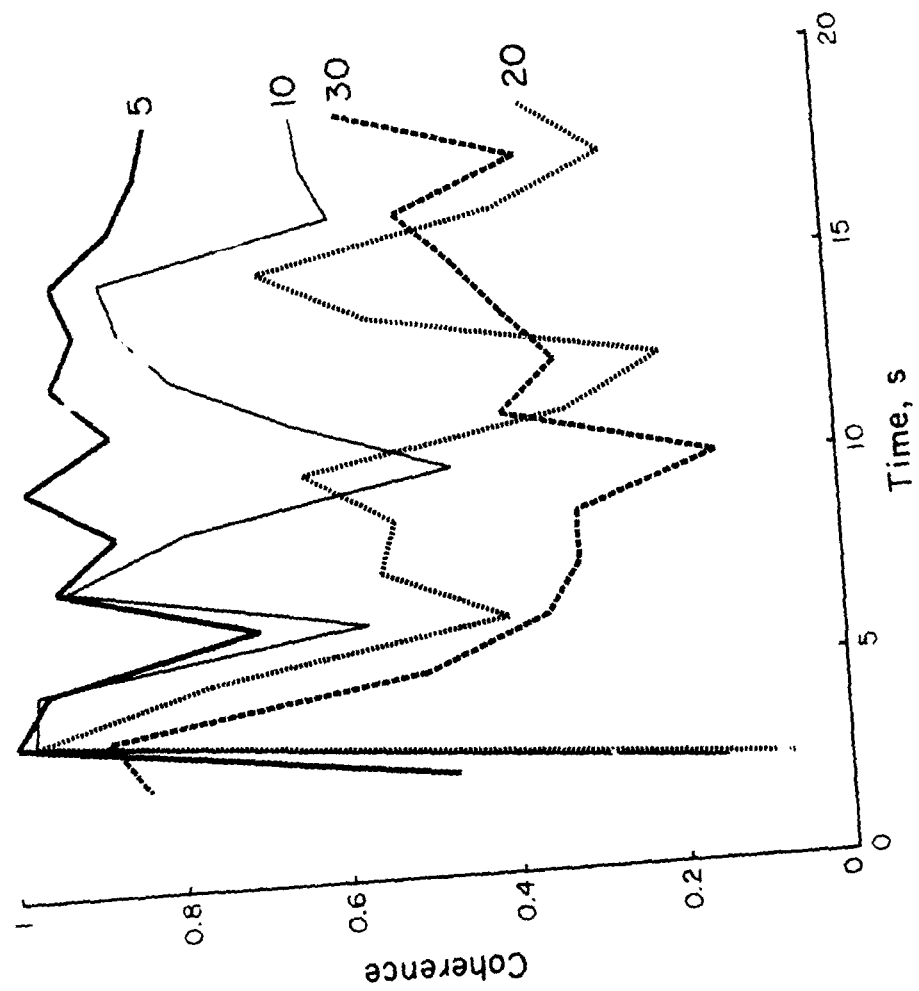


FIGURE 14

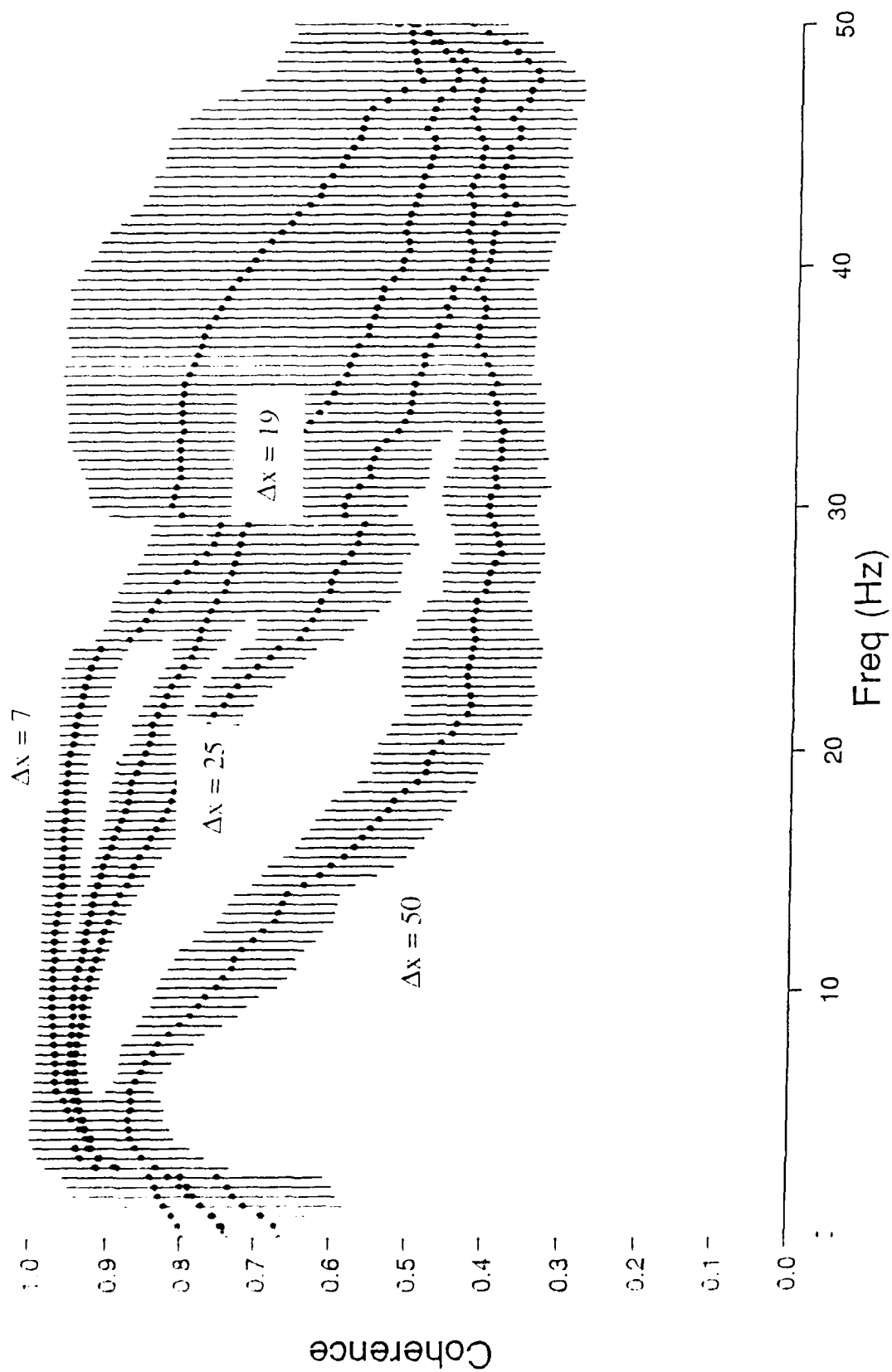


FIGURE 15

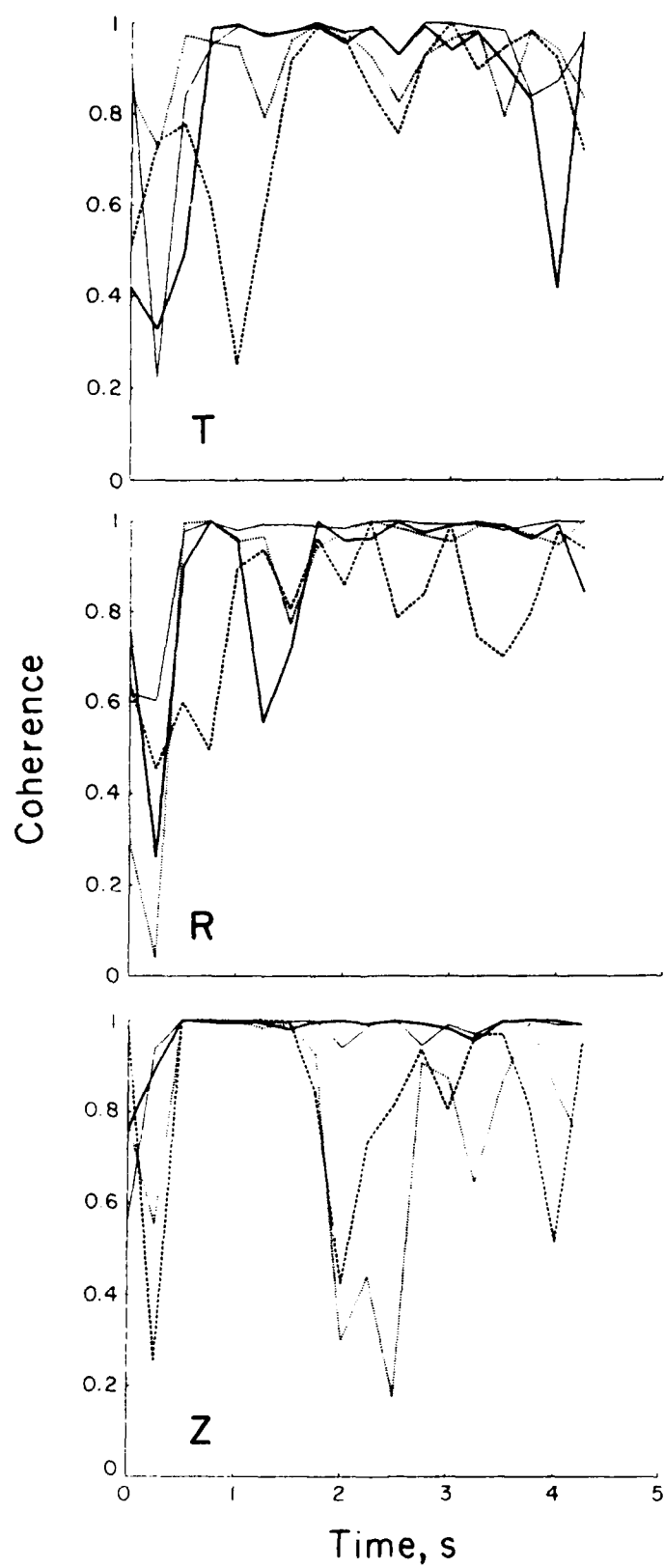


FIGURE 16

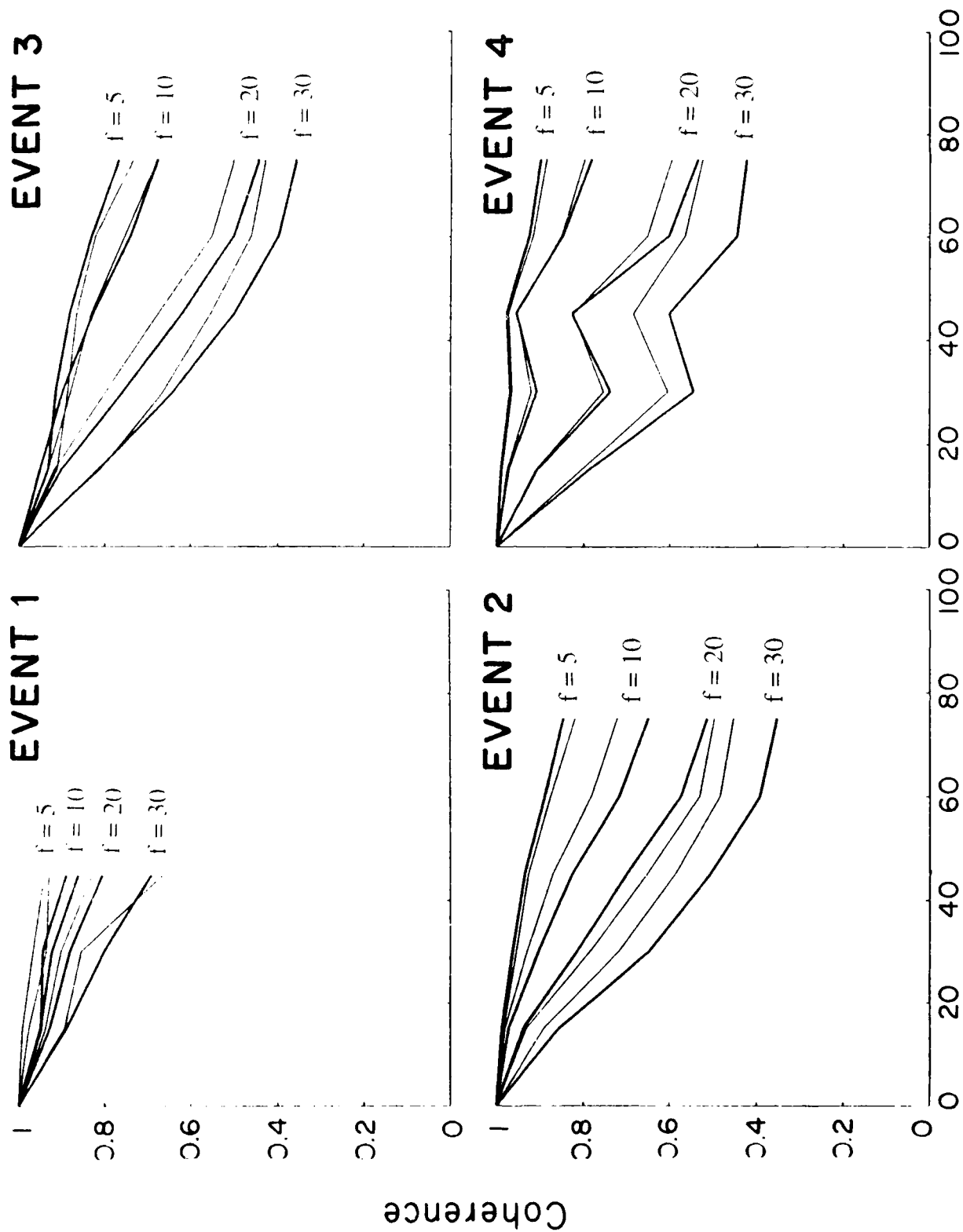


FIGURE 17

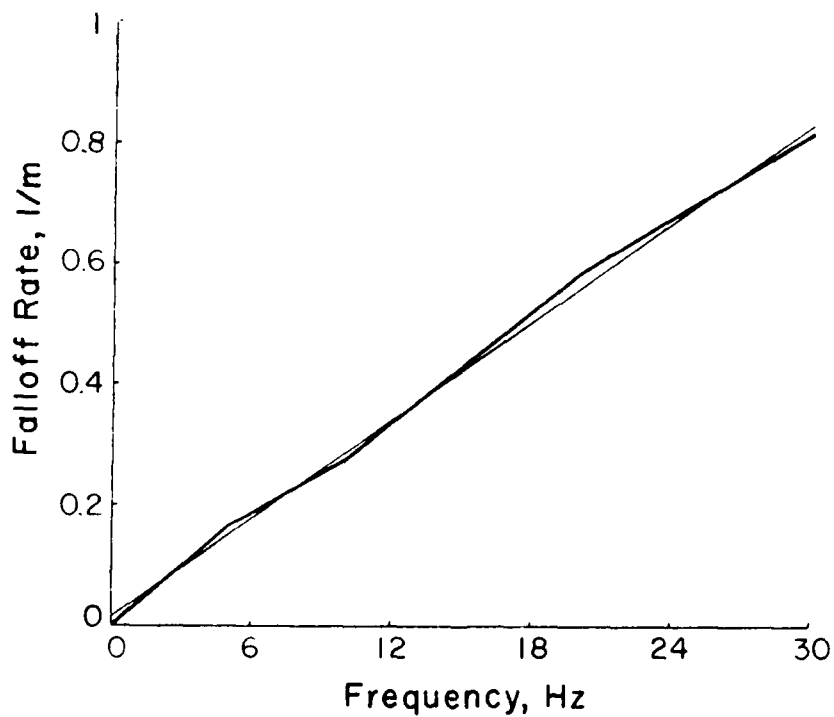
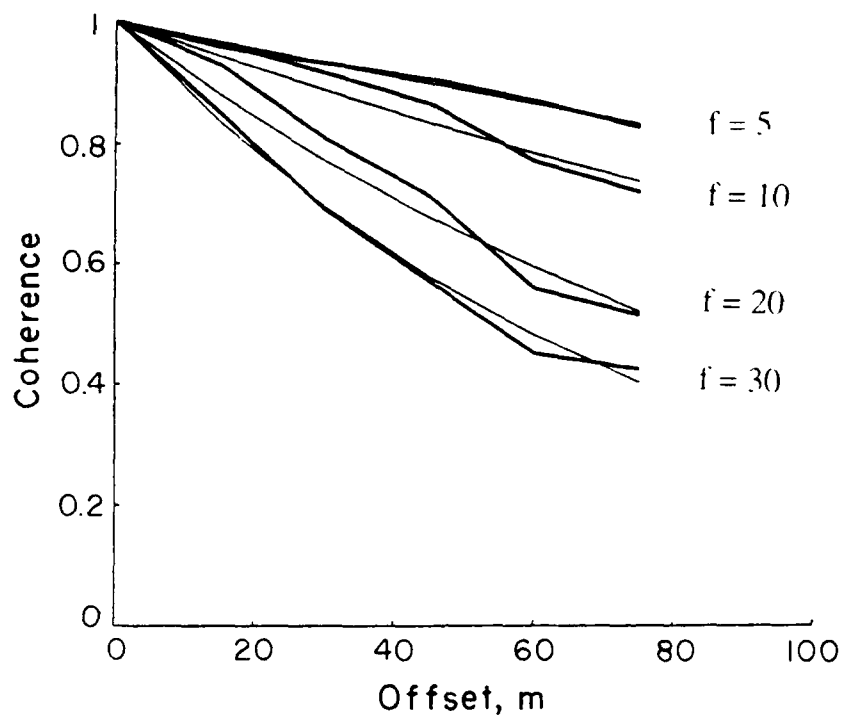


FIGURE 18

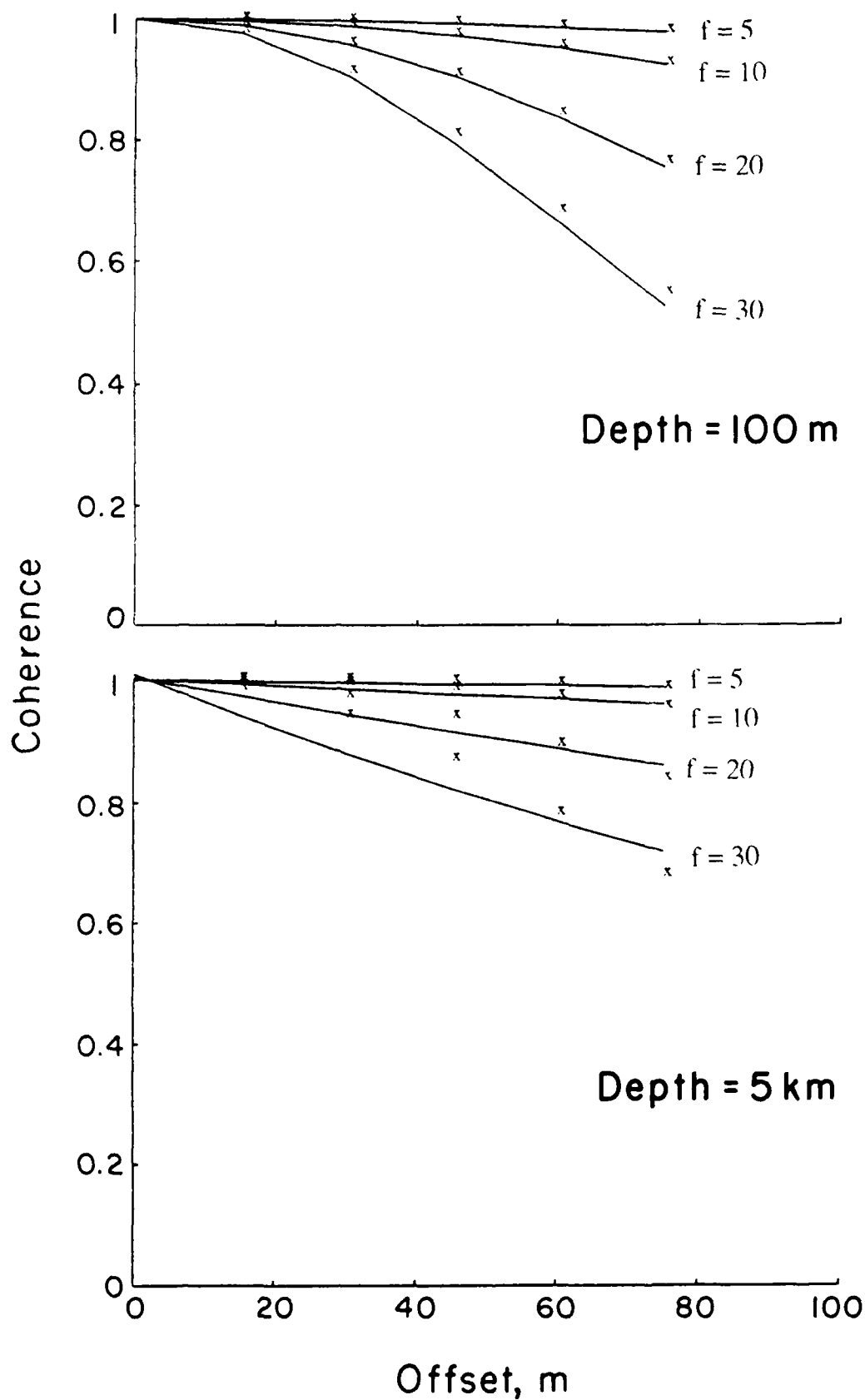


FIGURE 19

CONTRACTORS (United States)

Professor Keiiti Aki
Center for Earth Sciences
University of Southern California
University Park
Los Angeles, CA 90089-0741

Professor Thomas Ahrens
Seismological Lab, 252-21
Div. of Geological and Planetary
Sciences
California Institute of Technology
Pasadena, CA 91125

Professor Charles B. Archambeau
Cooperative Institute for Resch
in Environmental Sciences
University of Colorado
Boulder, CO 80309

Dr. Thomas C. Bache Jr.
Science Applications Int'l Corp.
10210 Campus Point Drive
San Diego, CA 92121 (2 copies)

Dr. Muawia Barazangi
Institute for the Study of
of the Continent
Cornell University
Ithaca, NY 14853

Dr. Douglas R. Baumgardt
Signal Analysis & Systems Div.
ENSCO, Inc.
5400 Port Royal Road
Springfield, VA 22151-2388

Dr. Jonathan Berger
Institute of Geophysics and
Planetary Physics
Scripps Institution of Oceanography
A-025
University of California, San Diego
La Jolla, CA 92093

Dr. S. Bratt
Science Applications Int'l Corp.
10210 Campus Point Drive
San Diego, CA 92121

Dr. Lawrence J. Burdick
Woodward-Clyde Consultants
P.O. Box 93245
Pasadena, CA 91109-3245 (2 copies)

Professor Robert W. Clayton
Seismological Laboratory/Div. of
Geological & Planetary Sciences
California Institute of Technology
Pasadena, CA 91125

Dr Karl Coyner
New England Research, Inc.
76 Olcott Drive
White River Junction, VT 05001

Dr. Vernon F. Cormier
Department of Geology & Geophysics
U-45, Room 207
The University of Connecticut
Storrs, Connecticut 06268

Dr. Steven Day
Dept. of Geological Sciences
San Diego State U.
San Diego, CA 92182

Dr. Zoltan A. Der
ENSCO, Inc.
5400 Port Royal Road
Springfield, VA 22151-2388

Professor John Ferguson
Center for Lithospheric Studies
The University of Texas at Dallas
P.O. Box 830688
Richardson, TX 75083-0688

Professor Stanley Flatte'
Applied Sciences Building
University of California,
Santa Cruz, CA 95064

Dr. Alexander Florence
SRI International
333 Ravenswood Avenue
Menlo Park, CA 94025-3493

Professor Steven Grand
University of Texas at Austin
Dept of Geological Sciences
Austin, TX 78713-7909

Dr. Henry L. Gray
Associate Dean of Dedman College
Department of Statistical Sciences
Southern Methodist University
Dallas, TX 75275

Professor Roy Greenfield
Geosciences Department
403 Deike Building
The Pennsylvania State University
University Park, PA 16802

Professor David G. Harkrider
Seismological Laboratory
Div of Geological & Planetary Sciences
California Institute of Technology
Pasadena, CA 91125

Professor Donald V. Helmberger
Seismological Laboratory
Div of Geological & Planetary Sciences
California Institute of Technology
Pasadena, CA 91125

Professor Eugene Herrin
Institute for the Study of Earth
and Man/Geophysical Laboratory
Southern Methodist University
Dallas, TX 75275

Professor Robert B. Herrmann
Department of Earth & Atmospheric
Sciences
Saint Louis University
Saint Louis, MO 63156

Professor Bryan Isacks
Cornell University
Dept of Geological Sciences
SNEE Hall
Ithaca, NY 14850

Professor Lane R. Johnson
Seismographic Station
University of California
Berkeley, CA 94720

Professor Thomas H. Jordan
Department of Earth, Atmospheric
and Planetary Sciences
Mass Institute of Technology
Cambridge, MA 02139

Dr. Alan Kafka
Department of Geology &
Geophysics
Boston College
Chestnut Hill, MA 02167

Professor Leon Knopoff
University of California
Institute of Geophysics
& Planetary Physics
Los Angeles, CA 90024

Professor Charles A. Langston
Geosciences Department
403 Deike Building
The Pennsylvania State University
University Park, PA 16802

Professor Thorne Lay
Department of Geological Sciences
1006 C.C. Little Building
University of Michigan
Ann Arbor, MI 48109-1063

Dr. Randolph Martin III
New England Research, Inc.
76 Olcott Drive
White River Junction, VT 05001

Dr. Gary McCartor
Mission Research Corp.
735 State Street
P.O. Drawer 719
Santa Barbara, CA 93102 (2 copies)

Professor Thomas V. McEvilly
Seismographic Station
University of California
Berkeley, CA 94720

Dr. Keith L. McLaughlin
S-CUBED,
A Division of Maxwell Laboratory
P.O. Box 1620
La Jolla, CA 92038-1620

Professor William Menke
Lamont-Doherty Geological Observatory
of Columbia University
Palisades, NY 10964

Professor Brian J. Mitchell
Department of Earth & Atmospheric
Sciences
Saint Louis University
Saint Louis, MO 63156

Mr. Jack Murphy
S-CUBED
A Division of Maxwell Laboratory
11800 Sunrise Valley Drive
Suite 1212
Reston, VA 22091 (2 copies)

Professor J. A. Orcutt
IGPP, A-205
Scripps Institute of Oceanography
Univ. of California, San Diego
La Jolla, CA 92093

Professor Keith Priestley
University of Nevada
Mackay School of Mines
Reno, NV 89557

Professor Paul G. Richards
Lamont-Doherty Geological
Observatory of Columbia Univ.
Palisades, NY 10964

Wilmer Rivers
Teledyne Geotech
314 Montgomery Street
Alexandria, VA 22314

Dr. Alan S. Ryall, Jr.
Center of Seismic Studies
1300 North 17th Street
Suite 1450
Arlington, VA 22209-2308 (4 copies)

Professor Charles G. Sammis
Center for Earth Sciences
University of Southern California
University Park
Los Angeles, CA 90089-0741

Professor Christopher H. Scholz
Geological Sciences
Lamont-Doherty Geological Observatory
Palisades, NY 10964

Dr. Jeffrey L. Stevens
S-CUBED,
A Division of Maxwell Laboratory
P.O. Box 1620
La Jolla, CA 92038-1620

Professor Brian Stump
Institute for the Study of Earth & Man
Geophysical Laboratory
Southern Methodist University
Dallas, TX 75275

Professor Ta-liang Teng
Center for Earth Sciences
University of Southern California
University Park
Los Angeles, CA 90089-0741

Dr. Clifford Thurber
State University of New York at
Stony Brooks
Dept of Earth and Space Sciences
Stony Brook, NY 11794-2100

Professor M. Nafi Toksoz
Earth Resources Lab
Dept of Earth, Atmospheric and
Planetary Sciences
Massachusetts Institute of Technology
42 Carleton Street
Cambridge, MA 02142

Professor Terry C. Wallace
Department of Geosciences
Building #77
University of Arizona
Tucson, AZ 85721

Weidlinger Associates
ATTN: Dr. Gregory Wojcik
4410 El Camino Real, Suite 110
Los Altos, CA 94022

Professor Francis T. Wu
Department of Geological Sciences
State University of New York
at Binghamton
Vestal, NY 13901

OTHERS (United States)

Dr. Monem Abdel-Gawad
Rockwell Internat'l Science Center
1049 Camino Dos Rios
Thousand Oaks, CA 91360

Professor Shelton S. Alexander
Geosciences Department
405 Deike Building
The Pennsylvania State University
University Park, PA 16802

Dr. Ralph Archuleta
Department of Geological
Sciences
Univ. of California at
Santa Barbara
Santa Barbara, CA

J. Barker
Department of Geological Sciences
State University of New York
at Binghamton
Vestal, NY 13901

Mr. William J. Best
907 Westwood Drive
Vienna, VA 22180

Dr. N. Biswas
Geophysical Institute
University of Alaska
Fairbanks, AK 99701

Dr. G. A. Bollinger
Department of Geological Sciences
Virginia Polytechnical Institute
21044 Derring Hall
Blacksburg, VA 24061

Mr. Roy Burger
1221 Serry Rd.
Schenectady, NY 12309

Dr. Robert Burrige
Schlumberger-Doll Resch Ctr.
Old Quarry Road
Ridgefield, CT 06877

Science Horizons, Inc.
ATTN: Dr. Theodore Cherry
710 Encinitas Blvd., Suite 101
Encinitas, CA 92024 (2 copies)

Professor Jon F. Claerbout
Professor Amos Nur
Dept. of Geophysics
Stanford University
Stanford, CA 94305 (2 copies)
Dr. Anton W. Dainty
Earth Resources Lab
Massachusetts Institute of Technology
42 Carleton Street
Cambridge, MA 02142
Professor Adam Dziewonski
Hoffman Laboratory
Harvard University
20 Oxford St.
Cambridge, MA 02138

Professor John Ebel
Dept of Geology and Geophysics
Boston College
Chestnut Hill, MA 02167

Dr. Donald Forsyth
Dept of Geological Sciences
Brown University
Providence, RI 02912

Dr. Anthony Gangi
Texas A&M University
Department of Geophysics
College Station, TX 77843

Dr. Freeman Gilbert
Institute of Geophysics &
Planetary Physics
University of California, San Diego
P.O. Box 109
La Jolla, CA 92037

Mr. Edward Giller
Pacific Seirra Research Corp.
1401 Wilson Boulevard
Arlington, VA 22209

Dr. Jeffrey W. Given
Sierra Geophysics
11255 Kirkland Way
Kirkland, WA 98033

Rong Song Jin
Teledyne Geotech
314 Montgomery Street
Alexandria, Virginia 22314

Professor F.K. Lamb
University of Illinois at
Urbana-Champaign
Department of Physics
1110 West Green Street
Urbana, IL 61801

Dr. Arthur Lerner-Lam
Lamont-Doherty Geological Observatory
of Columbia University
Palisades, NY 10964

Dr. L. Timothy Long
School of Geophysical Sciences
Georgia Institute of Technology
Atlanta, GA 30332

Dr. Peter Malin
University of California at
Santa Barbara
Institute for Central Studies
Santa Barbara, CA 93106

Dr. George R. Mellman
Sierra Geophysics
11255 Kirkland Way
Kirkland, WA 98033

Dr. Bernard Minster
IGPP, A-205
Scripps Institute of Oceanography
Univ. of California, San Diego
La Jolla, CA 92093

Professor John Nabelek
College of Oceanography
Oregon State University
Corvallis, OR 97331

Dr. Geza Nagy
U. California, San Diego
Dept of Ames, M.S. B-010
La Jolla, CA 92093

Dr. Jack Oliver
Department of Geology
Cornell University
Ithaca, NY 14850

Dr. Robert Phinney/Dr. F. A. Dahlen
Dept of Geological
Geological Science University
Princeton University
Princeton, NJ 08540

RADIX System, Inc.
Attn: Dr. Jay Pulli
2 Taft Court, Suite 203
Rockville, Maryland 20850

Dr. Norton Rimer
S-CUBED
A Division of Maxwell Laboratory
P.O. 1620
La Jolla, CA 92038-1620

Professor Larry J. Ruff
Department of Geological Sciences
1006 C.C. Little Building
University of Michigan
Ann Arbor, MI 48109-1063

Dr. Richard Sailor
TASC Inc.
55 Walkers Brook Drive
Reading, MA 01867

Thomas J. Sereno, Jr.
Science Application Int'l Corp.
10210 Campus Point Drive
San Diego, CA 92121

Dr. David G. Simpson
Lamont-Doherty Geological Observ.
of Columbia University
Palisades, NY 10964

Dr. Bob Smith
Department of Geophysics
University of Utah
1400 East 2nd South
Salt Lake City, UT 84112

Dr. S. W. Smith
Geophysics Program
University of Washington
Seattle, WA 98195

Dr. Stewart Smith
IRIS Inc.
1616 N. Fort Myer Drive
Suite 1440
Arlington, VA 22209

Rondout Associates
ATTN: Dr. George Sutton,
Dr. Jerry Carter, Dr. Paul Pomeroy
P.O. Box 224
Stone Ridge, NY 12484 (4 copies)

Dr. L. Sykes
Lamont Doherty Geological Observ.
Columbia University
Palisades, NY 10964

Dr. Pradeep Talwani
Department of Geological Sciences
University of South Carolina
Columbia, SC 29208

Dr. R. B. Tittmann
Rockwell International Science Center
1049 Camino Dos Rios
P.O. Box 1085
Thousand Oaks, CA 91360

Professor John H. Woodhouse
Hoffman Laboratory
Harvard University
20 Oxford St.
Cambridge, MA 02138

Dr. Gregory B. Young
ENSCO, Inc.
5400 Port Royal Road
Springfield, VA 22151-2588

FOREIGN (OTHERS)

Dr. Peter Basham
Earth Physics Branch
Geological Survey of Canada
1 Observatory Crescent
Ottawa, Ontario
CANADA K1A 0Y3

Professor Ari Ben-Menahem
Dept of Applied Mathematics
Weizman Institute of Science
Rehovot
ISRAEL 951729

Dr. Eduard Berg
Institute of Geophysics
University of Hawaii
Honolulu, HI 96822

Dr. Michel Bouchon - Universite
Scientifique et Medicale de Grenoble
Lab de Geophysique - Interne et
Tectonophysique - I.R.I.G.M-B.P.
38402 St. Martin D'Heres
Cedex FRANCE

Dr. Hilmar Bungum/NTNF/NORSAR
P.O. Box 51
Norwegian Council of Science,
Industry and Research, NORSAR
N-2007 Kjeller, NORWAY

Dr. Michel Campillo
I.R.I.G.M.-B.P. 68
38402 St. Martin D'Heres
Cedex, FRANCE

Dr. Kin-Yip Chun
Geophysics Division
Physics Department
University of Toronto
Ontario, CANADA M5S 1A7

Dr. Alan Douglas
Ministry of Defense
Blacknest, Brimpton,
Reading RG7-4RS
UNITED KINGDOM

Dr. Manfred Henger
Fed. Inst. For Geosciences & Nat'l Res.
Postfach 510153
D-3000 Hannover 51
FEDERAL REPUBLIC OF GERMANY

Ms. Eva Johannisson
Senior Research Officer
National Defense Research Inst.
P.O. Box 27322
S-102 54 Stockholm
SWEDEN

Tormod Kvaerna
NTNF/NORSAR
P.O. Box 51
N-2007 Kjeller, NORWAY

Mr. Peter Marshall, Procurement
Executive, Ministry of Defense
Blacknest, Brimpton,
Reading FG7-4RS
UNITED KINGDOM (3 copies)

Dr. Robert North
Geophysics Division
Geological Survey of Canada
1 Observatory crescent
Ottawa, Ontario
CANADA, K1A 0Y3

Dr. Frode Ringdal
NTNF/NORSAR
P.O. Box 51
N-2007 Kjeller, NORWAY

Dr. Jorg Schlittenhardt
Federal Inst. for Geosciences & Nat'l Res.
Postfach 510153
D-3000 Hannover 51
FEDERAL REPUBLIC OF GERMANY

University of Hawaii
Institute of Geophysics
ATTN: Dr. Daniel Walker
Honolulu, HI 96822

FOREIGN CONTRACTORS

Dr. Ramon Cabre, S.J.
Observatorio San Calixto
Casilla 5939
La Paz Bolivia

Professor Peter Harjes
Institute for Geophysik
Rhur University/Bochum
P.O. Box 102148, 4630 Bochum 1
FEDERAL REPUBLIC OF GERMANY

Dr. E. Husebye
NTNF/NORSAR
P.O. Box 51
N-2007 Kjeller, NORWAY

Professor Brian L.N. Kennett
Research School of Earth Sciences
Institute of Advanced Studies
G.P.O. Box 4
Canberra 2601
AUSTRALIA

Dr. B. Massinon
Societe Radiomana
27, Rue Claude Bernard
7,005, Paris, FRANCE (2 copies)

Dr. Pierre Mechler
Societe Radiomana
27, Rue Claude Bernard
75005, Paris, FRANCE

Dr. Svein Mykkeltveit
NTNF/NORSAR
P.O. Box 51
N-2007 Kjeller, NORWAY (3 copies)

GOVERNMENT

Dr. Ralph Alewine III
DARPA/NMRO
1400 Wilson Boulevard
Arlington, VA 22209-2308

Dr. Robert Blandford
DARPA/NMRO
1400 Wilson Boulevard
Arlington, VA 22209-2308

Sandia National Laboratory
ATTN: Dr. H. B. Durham
Albuquerque, NM 87185

Dr. Jack Evernden
USGS-Earthquake Studies
345 Middlefield Road
Menlo Park, CA 94025

U.S. Geological Survey
ATTN: Dr. T. Hanks
Nat'l Earthquake Resch Center
345 Middlefield Road
Menlo Park, CA 94025

Dr. James Hannon
Lawrence Livermore Nat'l Lab.
P.O. Box 808
Livermore, CA 94550

Paul Johnson
ESS-4, Mail Stop J979
Los Alamos National Laboratory
Los Alamos, NM 87545

Ms. Ann Kerr
DARPA/NMRO
1400 Wilson Boulevard
Arlington, VA 22209-2308

Dr. Max Koontz
US Dept of Energy/DP 5
Forrestal Building
1000 Independence Ave.
Washington, D.C. 20585

Dr. W. H. K. Lee
USGS
Office of Earthquakes, Volcanoes,
& Engineering
Branch of Seismology
345 Middlefield Rd
Menlo Park, CA 94025

Dr. William Leith
U.S. Geological Survey
Mail Stop 928
Reston, VA 22092

Dr. Richard Lewis
Dir. Earthquake Engineering and
Geophysics
U.S. Army Corps of Engineers
Box 631
Vicksburg, MS 39180

Dr. Robert Masse'
Box 25046, Mail Stop 967
Denver Federal Center
Denver, Colorado 80225

Richard Morrow
ACDA/VI
Room 5741
320 21st Street N.W.
Washington, D.C. 20451

Dr. Keith K. Nakanishi
Lawrence Livermore National Laboratory
P.O. Box 808, L-205
Livermore, CA 94550 (2 copies)

Dr. Carl Newton
Los Alamos National Lab.
P.O. Box 1663
Mail Stop C335, Group ESS-3
Los Alamos, NM 87545

Dr. Kenneth H. Olsen
Los Alamos Scientific Lab.
P.O. Box 1663
Mail Stop C335, Group ESS-3
Los Alamos, NM 87545

Howard J. Patton
Lawrence Livermore National
Laboratory
P.O. Box 808, L-205
Livermore, CA 94550

Mr. Chris Paine
Office of Senator Kennedy
SR 315
United States Senate
Washington, D.C. 20510

AFOSR/NP
ATTN: Colonel Jerry J. Perrizo
Bldg 410
Bolling AFB, Wash D.C. 20332-6448

HQ AFTAC/TT
Attn: Dr. Frank F. Pilotte
Patrick AFB, Florida 32925-6001

Mr. Jack Rachlin
USGS - Geology, Rm 3 C136
Mail Stop 928 National Center
Reston, VA 22092

Robert Reinke
AFWL/NTESS
Kirtland AFB, NM 87117-6008

Dr. Byron Ristvet
HQ DNA, Nevada Operations Office
Attn: NVCG
P.O. Box 98539
Las Vegas, NV 89193

HQ AFTAC/TGR
Attn: Dr. George H. Rothe
Patrick AFB, Florida 32925-6001

Donald L. Springer
Lawrence Livermore National Laboratory
P.O. Box 808, L-205
Livermore, CA 94550

Dr. Lawrence Turnbull
OSWR/NED
Central Intelligence Agency
CIA, Room 5G48
Washington, D.C. 20505

Dr. Thomas Weaver
Los Alamos National Laboratory
P.O. Box 1663
MS C 335
Los Alamos, NM 87545

GL/SULL
Research Library
Hanscom AFB, MA 01731-5000 (2 copies)

Secretary of the Air Force (SAFRD)
Washington, DC 20330
Office of the Secretary Defense
DDR & E
Washington, DC 20330

HQ DNA
ATTN: Technical Library
Washington, DC 20305

DARPA/RMO/RETRIEVAL
1400 Wilson Blvd.
Arlington, VA 22209

DARPA/RMO/Security Office
1400 Wilson Blvd.
Arlington, VA 22209

GL/XO
Hanscom AFB, MA 01731-5000

GL/LW
Hanscom AFB, MA 01731-5000

DARPA/PM
1400 Wilson Boulevard
Arlington, VA 22209

Defense Technical
Information Center
Cameron Station
Alexandria, VA 22314
(5 copies)

Defense Intelligence Agency
Directorate for Scientific &
Technical Intelligence
Washington, D.C. 20301

Defense Nuclear Agency/SPSS
ATTN: Dr. Michael Shore
6801 Telegraph Road
Alexandria, VA 22310

AFTAC/CA (STINFO)
Patrick AFB, FL 32925-6001

TACTEC
Battelle Memorial Institute
505 King Avenue
Columbus, OH 43201 (Final report only)

Mr. Alfred Lieberman
ACDA/VI-0A State Department Building
Room 5726
320 - 21st Street, NW
Washington, D.C. 20451